Available online at www.sciencedirect.com

ScienceDirect

Geochimica et Cosmochimica Acta 265 (2019) 259–278

Geochimica et Cosmochimica Acta

www.elsevier.com/locate/gca

Mineralogy and petrology of Dominion Range 08006: A very primitive CO3 carbonaceous chondrite

Jemma Davidson [a,*,1], Conel M.O'D. Alexander [a], Rhonda M. Stroud [b] Henner Busemann [c], Larry R. Nittler [a]

[a] *Department of Terrestrial Magnetism, Carnegie Institution of Washington, 5241 Broad Branch Road, Washington DC 20015-1305, USA*
[b] *Naval Research Laboratory Code 6366, 4555 Overlook Ave. SW, Washington DC 20375, USA*
[c] *Institute of Geochemistry and Petrology, ETH Zürich, Clausiusstrasse 25, 8092 Zürich, Switzerland*

Received 20 June 2019; accepted in revised form 27 August 2019; available online 5 September 2019

Abstract

Here we report the relative degrees of thermal metamorphism for five Antarctic Ornans-like carbonaceous (CO) chondrites, including Dominion Range (DOM) 08006, as determined from the Cr-content of their FeO-rich (ferroan) olivine. These five CO3 chondrites complete the previously poorly-defined CO3.00 to 3.2 chondrite metamorphic trend. DOM 08006 appears to be a highly primitive CO chondrite of petrologic type 3.00. We report the detailed mineralogy and petrography of DOM 08006 using a coordinated, multi-technique approach.

The interchondrule matrix in DOM 08006 consists of unequilibrated mixtures of silicate, metal, and sulfide minerals and lacks Fe-rich rims on silicates indicating that DOM 08006 has only experienced minimal, if any, thermal metamorphism. This is also reflected by the Co/Ni ratios of Ni-rich and Ni-poor metal, a sensitive indicator of thermal metamorphism, and the presence of euhedral chrome-spinel grains, which typically become subhedral to anhedral during progressive metamorphism. DOM 08006 matrix shows minor evidence for aqueous alteration and while the presence of magnetite surrounding metal in chondrules indicates that there has been some interaction with fluid, much metal remains and none of the sulfides analyzed show evidence of being formed by aqueous alteration. Furthermore, the plagioclase of ~50% of chondrules analyzed show resolvable excess silica indicating that these chondrules have experienced minimal, if any, reprocessing in the CO parent body.

Noble gas data for DOM 08006 show that it contains the highest concentrations of trapped ^{36}Ar and ^{132}Xe of all CO chondrites analyzed to date, further indicating that DOM 08006 is the most primitive CO chondrite known. The cosmic ray exposure age of DOM 08006 is estimated to be ~19 Ma.

The minimally altered nature of DOM 08006 demonstrates that it is an extremely important sample for providing valuable insight into early Solar System conditions. At a total weight of 667 g, a significant amount of material is available for a wide array of future studies.
© 2019 Elsevier Ltd. All rights reserved.

Keywords: CO chondrites; DOM 08006; Primitive meteorites; Thermal metamorphism

1. INTRODUCTION

After interplanetary dust particles, carbonaceous chondrites provide some of the most primitive extraterrestrial samples available for study. Chondrites that have experienced only minor parent body processing (i.e., aqueous

* Corresponding author.
E-mail address: jdavidson@asu.edu (J. Davidson).
[1] Current address: Center for Meteorite Studies, School of Earth and Space Exploration, Arizona State University, 781 East Terrace Road, Tempe, AZ 85287-6004, USA.

https://doi.org/10.1016/j.gca.2019.08.032
0016-7037/© 2019 Elsevier Ltd. All rights reserved.

alteration and/or thermal metamorphism) typically contain abundant presolar grains (e.g., Nguyen et al., 2007; Floss and Stadermann, 2009; Davidson et al., 2014a; Nittler et al., 2018), isotopically anomalous organic matter (e.g., Busemann et al., 2006; Alexander et al., 2007, 2012, 2013), and abundant amorphous silicates in their matrices (e.g., Abreu and Brearley, 2010; Howard et al., 2015). Thus, they can provide valuable insight into early Solar System conditions, and the evolution of early Solar System materials as the result of nebular and parent body processes. The petrologic type 3 Ornans-like carbonaceous (CO3) chondrites exhibit the complete metamorphic sequence from type 3.0 to 3.9 (McSween, 1977; Sears et al., 1980). For the least altered type 3 chondrites, the Cr-content of ferroan olivine has been shown to be a very sensitive probe of the degree of thermal metamorphism experienced (Grossman and Brearley, 2005), making it possible to subdivide the types between 3.00 and 3.2, and identify the most primitive samples. This technique has been applied to the ordinary chondrites (OC) (Grossman and Brearley, 2005), the Renazzo-like carbonaceous (CR) chondrites (Davidson et al., 2015; Davidson et al., 2019; Schrader et al., 2015), and the Mighei-like carbonaceous (CM) chondrites (Schrader and Davidson, 2017). It has also been applied to the CO chondrites, but they follow a distinct trend that, to date, is less well defined largely because there are so few known type 3.00–3.2 members of this group (Grossman and Brearley, 2005).

Recent searches of the Dominion Range (DOM) and Miller Range (MIL) ice fields have recovered significant numbers of primitive (i.e., little to no evidence of parent body aqueous alteration and/or thermal metamorphism) CO3s. Of these, DOM 08006 appears to be one of the least aqueously altered and thermally metamorphosed chondrites known. The first hint that this might be the case came from a study of the amino acids in ureilites and Vigarano-like (CV) and CO chondrites that showed that DOM 08006 contains lower absolute and relative abundances of straight-chain amino acids than the most primitive CO identified to date, Allan Hills (ALH) 77307 (Burton et al., 2012). These amino acids are produced during thermal alteration, suggesting that DOM 08006 might have experienced less thermal metamorphism than ALH 77307. This prompted an *in situ* NanoSIMS O-, C-, and N-isotopic survey of DOM 08006 that revealed an extremely high abundance of presolar silicates in its matrix, higher than any other chondrite (including ALH 77307) and comparable with interplanetary dust particles (Nittler et al., 2013, 2018). As presolar silicate grains are extremely sensitive indicators of both parent body aqueous alteration and thermal metamorphism (e.g., Zinner, 2014 and references therein), this high abundance indicates that DOM 08006 is indeed very primitive (Nittler et al., 2013, 2018). Subsequent bulk analyses showed that DOM 08006 also has a higher bulk C content, and heavier bulk N- and H-isotopic compositions than ALH 77307 (Alexander et al., 2014, 2018). Since bulk C contents, and D and ^{15}N isotopic enrichments are typically associated with insoluble organic matter (IOM) (e.g., Busemann et al., 2006) whose structure, abundance and elemental/isotopic compositions can be sensitive indicators of the degree of thermal metamorphism (e.g., Alexander et al., 2007, 2010; Bonal et al., 2007, 2016), these results again suggested that DOM 08006 may be more primitive than ALH 77307.

We present here detailed petrographic observations of DOM 08006 as well as the Cr-content of ferroan olivine in four other primitive Antarctic CO3 chondrites to better define the CO metamorphic trend. We also discuss the noble gases present in bulk DOM 08006 and its IOM to assess the degree of primitiveness of this meteorite. Preliminary data were presented in Davidson et al. (2014b). Our observations agree with presolar grain abundances (Nittler et al., 2018), and the isotopic compositions (Alexander et al., 2018) and Raman spectral parameters (Bonal et al., 2016) of IOM, providing further support that DOM 08006 is at least as primitive as ALH 77307, and is likely the most primitive CO3 known.

2. ANALYTICAL PROCEDURE

2.1. Sample selection and summary

Five samples (DOM 08006, DOM 10104, MIL 05024, MIL 090010, and MIL 090470) were selected for study as they had been previously identified as potentially very primitive CO3 chondrites based on their bulk and IOM isotopic compositions and bulk mineralogies as determined by position sensitive X-ray diffraction (Alexander et al., 2018).

MIL 090010 and MIL 090470 are part of a very large MIL 07099 pairing group, along with 55 other CO3 chondrites. MIL 05024 is a member of the large MIL 03377 pairing group. Both the MIL 07099 and MIL 03377 pairing groups may be related (Alexander et al., 2018). DOM 08006 has been linked with the DOM 08004 pairing group, but based on bulk H, C and N abundances Alexander et al. (2018) concluded that DOM 08006 does not belong to this slightly more metamorphosed pairing group. Although, DOM 08004 has not been studied here, another member of the pairing group, DOM 10104, has been.

2.2. Mineralogy and petrology analyses

Polished thin sections of DOM 08006,16, DOM 10104,15, MIL 05024,15, MIL 090010,9, and MIL 090470,9 were initially characterized with an optical microscope before they were carbon coated for electron microscopy. Full thin section backscattered electron (BSE) images and X-ray element maps were then obtained with the JEOL JSM-6500F field emission scanning electron microscope (FE-SEM) at the Carnegie Institution of Washington (CIW) (operating conditions: 15.0 kV and ~1 nA). These maps show the elemental and mineralogical distributions within the samples, and were used to identify mineral phases for further study, including FeO-rich (ferroan) olivine (Suppl. Figs. 1 and 2). High-resolution BSE and secondary electron images were obtained for each chondrule selected for study. Modal abundances of different phases within DOM 08006 were determined from a full thin section BSE image using Adobe Photoshop® and from BSE images of individual chondrules using ImageJ (Schneider

Table 1
Mean compositions and standard deviations of ferroan chondrule olivine (wt.%) in CO and ungrouped chondrites.

Meteorite	N	MgO	Al_2O_3	SiO_2	P_2O_5	CaO	TiO_2	Cr_2O_3	MnO	FeO	Na_2O	NiO	Total	Fa (mol%)
CO3 chondrites														
DOM 08006	54	33.3 ± 6.7	0.04 ± 0.02	36.6 ± 1.5	na	0.19 ± 0.07	bdl	0.36 ± 0.06	0.29 ± 0.09	29.4 ± 8.1	bdl	bdl	100.2	33.6 ± 10.8
DOM 10104	60	29.5 ± 5.9	0.08 ± 0.20	35.6 ± 1.4	na	0.26 ± 0.18	bdl	0.26 ± 0.11	0.35 ± 0.10	34.5 ± 7.0	bdl	bdl	100.8	40.0 ± 9.8
MIL 05024	51	30.4 ± 5.5	0.06 ± 0.12	36.1 ± 1.3	na	0.22 ± 0.11	bdl	0.23 ± 0.10	0.33 ± 0.07	34.1 ± 6.6	bdl	bdl	101.5	52.6 ± 9.4
MIL 090010	57	27.6 ± 6.8	0.03 ± 0.03	35.8 ± 3.2	na	0.23 ± 0.13	bdl	0.21 ± 0.09	0.38 ± 0.09	36.5 ± 8.0	bdl	bdl	100.9	43.1 ± 11.5
MIL 090470	52	29.7 ± 5.7	0.04 ± 0.03	35.8 ± 1.3	na	0.20 ± 0.08	bdl	0.23 ± 0.09	0.35 ± 0.08	34.8 ± 7.1	bdl	bdl	101.2	40.0 ± 9.6
ALH 77307[a]	45	32.2 ± 5.4	0.04 ± 0.02	36.4 ± 1.2	0.02 ± 0.03	0.24 ± 0.12	0.03 ± 0.03	0.38 ± 0.07	0.31 ± 0.08	27.3 ± 6.4	na	na	96.9	32.5 ± 8.8
Y-81020[a]	39	32.7 ± 7.2	0.04 ± 0.03	36.5 ± 1.6	0.04 ± 0.04	0.23 ± 0.11	0.02 ± 0.03	0.33 ± 0.13	0.33 ± 0.13	27.3 ± 8.3	na	na	97.5	32.5 ± 11.9
Colony[a]	27	28.6 ± 9.9	0.05 ± 0.05	36.1 ± 2.2	0.04 ± 0.04	0.20 ± 0.07	0.01 ± 0.02	0.31 ± 0.13	0.36 ± 0.10	32.1 ± 11.4	na	na	97.7	39.8 ± 15.5
Rainbow[a]	49	30.9 ± 6.0	0.04 ± 0.02	36.6 ± 1.3	0.03 ± 0.04	0.18 ± 0.07	0.01 ± 0.02	0.08 ± 0.05	0.32 ± 0.08	31.0 ± 7.0	na	na	99.1	36.5 ± 10.2
Kainsaz[a]	41	34.2 ± 7.1	0.04 ± 0.03	37.0 ± 1.6	0.03 ± 0.05	0.16 ± 0.08	0.02 ± 0.03	0.09 ± 0.06	0.28 ± 0.08	26.5 ± 8.1	na	na	98.4	30.9 ± 11.1
DOM 03238[b]		–	–	–	–	–	–	0.27 ± 0.18	–	–	–	–	–	–
Ungrouped chondrites														
Acfer 094[a]	40	32.7 ± 4.4	0.04 ± 0.03	36.8 ± 1.1	0.05 ± 0.08	0.30 ± 0.12	0.02 ± 0.02	0.34 ± 0.10	0.33 ± 0.07	28.5 ± 4.9	na	na	99.1	33.1 ± 7.0
MIL 07687[c]	52	34.3 ± 4.5	0.06 ± 0.06	36.7 ± 1.1	na	0.25 ± 0.10	bdl	0.35 ± 0.11	0.31 ± 0.08	28.5 ± 5.6	bdl	bdl	100.5	32.0 ± 7.0

na = not analyzed, bdl = below detection limit.
[a] Grossman and Brearley (2005).
[b] Grossman and Rubin (2006).
[c] Davidson et al. (2014b).

et al., 2012). Apparent chondrule diameters were determined by measuring the major and minor axes of chondrules in BSE images with Adobe Photoshop®.

Major and minor element abundances (Na, Fe, Si, Ni, Ca, Mg, Cr, Al, Mn, and Ti for silicate phases, chrome-spinel and magnetite; P, Fe, Si, Ni, S, Co, Cu, and Cr for metal and sulfide phases) were determined quantitatively with a five-spectrometer wavelength dispersive JEOL 8900 electron microprobe analyzer (EMPA) at CIW. The thin sections were analyzed with a ~1 μm, 30 nA focused beam and a 15 kV accelerating voltage. Data reduction was carried out using a Phi-Rho-Z correction method. For most elements, the on-peak counting times were 30 seconds, with 15 seconds on each background for a total of 60 seconds per element. The exceptions were Cr, Al, Mn, and Ti for silicate and magnetite analyses, and P, Co, Si, Cu, and Cr for metal and sulfide analyses, for which on-peak counting times were 60 seconds, and each background was 30 seconds for a total of 120 seconds per element.

Only metal, sulfide, stoichiometric olivine, pyroxene, and plagioclase analyses with totals between 98–102 wt.% were retained and are presented here (Tables 1–3). Detection limits (in wt.%) and standards used are listed in Table 2 for silicate analyses and Table 3 for metal and sulfide analyses.

2.3. FIB-TEM analyses

Five matrix sections for transmission electron microscopy (TEM) were extracted from DOM 08006 by means of a focused ion beam (FIB) lift-out technique with an FEI Nova 600 FIB-SEM equipped with an Ascend Extreme Access micromanipulator at the Naval Research Laboratory (NRL). Section locations were chosen to include presolar grains identified by NanoSIMS mapping (Nittler et al., 2018); Pt fiducial marks were first laid down by electron beam deposition to indicate the presolar grain locations within the sections. The entire 8–10 μm length of each FIB section was covered with a C strap by ion beam deposition to protect the sample during milling. Subsequent analytical TEM studies were performed with a JEOL JEM 2200FS field-emission scanning TEM at NRL, equipped with a Noran System Six energy dispersive X-ray spectrometer. Energy-dispersive X-ray spectroscopy (EDS) spectra of individual grains were quantified with Cliff-Lorimer routines, with laboratory K factors calibrated from San Carlos olivine and Tanzanian hibonite standards, and instrument default K factors for C and S (Stroud et al., 2013).

2.4. Noble gas analyses

All noble gas isotopes (He–Xe) were analyzed at ETH Zurich in a bulk DOM 08006 sample (5.35 ± 0.03 mg) and IOM residue extracted from another bulk sample (0.82 ± 0.01 mg). See Alexander et al. (2018) for details regarding IOM sample preparation. Both samples were extracted by fusion in one step at ~1700 °C. Details of the experiments are described by Riebe et al. (2017). Blank corrections were <1% for all isotopes in both samples, except for ^{22}Ne (1.5%) and ^{40}Ar (62%) in the IOM sample.

Table 2
Representative silicate analyses in ferromagnesian chondrules and matrix grains in DOM 08006,16.

Chondrules													Matrix				
Chondrule/Grain[a]	**Ch6**	**Ch12**	**Ch2**	**Ch21**	**Ch14**	**Ch1**	**Ch19**	**Ch5**	**Ch8**	**Ch5**	**Ch5**	**Ch7**	**G25**	**G43**	**G44**	**G5**	**G32**
Chondrule Type[b]	**I**	**I**	**II**	**II**	**II**	**I**	**I**	**I**	**I**	**I**	**I**	**I**					
Silicate Type[c]	**Ol**	**Ol**	**Ol**	**Ol**	**Ol Rel.**	**L-Ca Px**	**L-Ca Px**	**H-Ca Px**	**H-Ca Px**	**Plag**	**Plag**	**Plag**	**Ol**	**Ol**	**Rel. Ol**	**L-Ca Px**	**H-Ca Px**
Chemical composition (wt.%)																	
SiO_2	42.0	41.9	36.4	39.4	41.8	58.1	56.6	49.3	55.1	54.6	55.1	46.2	32.0	34.6	41.0	50.8	48.7
TiO_2	bdl	bdl	bdl	bdl	bdl	0.23	0.15	1.29	0.68	0.32	0.31	0.04	bdl	bdl	0.04	0.04	0.14
Al_2O_3	bdl	bdl	0.05	0.05	0.03	1.13	1.60	8.23	2.56	23.89	24.45	32.74	bdl	0.04	0.07	0.47	1.30
Cr_2O_3	0.49	0.71	0.41	0.33	0.39	0.41	1.11	1.09	0.87	0.28	0.08	bdl	0.51	0.33	0.32	0.80	0.93
FeO	0.70	0.95	32.04	13.82	2.70	0.61	4.02	0.26	1.01	0.34	0.21	0.09	54.50	40.50	5.07	28.30	28.52
MnO	0.26	0.90	0.33	0.14	0.16	0.07	0.23	0.25	0.17	0.22	0.20	bdl	0.63	0.35	0.08	0.34	0.36
MgO	56.4	55.2	30.9	45.6	55.1	38.5	34.7	18.1	30.5	4.3	3.6	1.1	12.7	23.6	52.4	17.6	10.3
CaO	0.22	0.16	0.21	0.15	0.23	0.43	1.66	20.42	7.82	12.86	12.52	18.81	0.14	0.21	0.22	0.92	7.79
NiO	bdl	bdl	bdl	bdl	bdl	bdl	bdl	bdl	0.31	bdl	bdl	bdl	bdl	0.07	bdl	bdl	bdl
Na_2O	bdl	bdl	bdl	bdl	bdl	bdl	bdl	bdl	bdl	2.47	3.30	0.26	bdl	bdl	bdl	bdl	0.16
Total	0.00	99.82	0.00	99.48	0.00	0.00	100.03	98.94	98.99	99.29	99.76	99.21	0.00	99.67	99.24	0.00	98.19
Cation formula based on 4 oxygens for olivine, 6 for pyroxene, and 8 for plagioclase																	
Si	0.990	0.994	0.992	0.991	0.991	1.963	1.945	1.784	1.924	2.490	2.501	2.144	0.986	0.994	0.993	1.970	1.961
Ti	bdl	bdl	bdl	bdl	bdl	0.006	0.004	0.035	0.018	0.011	0.010	0.001	bdl	bdl	0.001	0.001	0.004
Al	bdl	bdl	0.002	0.002	0.001	0.045	0.065	0.351	0.105	1.285	1.308	1.790	bdl	0.001	0.002	0.022	0.062
Cr	0.009	0.013	0.009	0.006	0.007	0.011	0.030	0.031	0.024	0.010	0.003	bdl	0.012	0.007	0.006	0.025	0.030
Fe	0.014	0.019	0.731	0.291	0.053	0.017	0.116	0.008	0.030	0.013	0.008	0.004	1.405	0.973	0.103	0.918	0.961
Mn	0.005	0.018	0.008	0.003	0.003	0.002	0.007	0.008	0.005	0.008	0.007	bdl	0.017	0.009	0.002	0.011	0.012
Mg	1.981	1.952	1.256	1.709	1.944	1.943	1.776	0.979	1.587	0.295	0.243	0.074	0.582	1.009	1.891	1.019	0.616
Ca	0.005	0.004	0.006	0.004	0.006	0.016	0.061	0.792	0.293	0.629	0.609	0.935	0.005	0.006	0.006	0.038	0.336
Ni	bdl	bdl	bdl	bdl	bdl	bdl	bdl	bdl	0.009	bdl	bdl	bdl	bdl	0.002	0.000	bdl	bdl
Na	bdl	bdl	bdl	bdl	bdl	bdl	bdl	bdl	bdl	0.219	0.290	0.024	bdl	bdl	bdl	bdl	0.013
Total	2.006	3.000	2.000	3.005	3.005	4.003	4.003	3.989	3.994	4.961	4.979	4.972	2.008	3.001	3.002	1.987	3.995
Fa	1	1	37	15	3								71	49	5		
Fo	99	99	63	85	97								29	51	95		
En						98	91	55	83							52	32
Fs						1	6	0	2							46	50
Wo						1	3	45	15							2	18
An										76	68	98					
Ab										24	32	2					

bdl = below detection limit.

Standards used for silicate analyses (with detection limits in wt.%) were forsterite for Si (0.03) and Mg (0.02), cossyrite for Ti (0.03) and Na (0.03), spessartine for Al (0.01) and Mn (0.03), chromite for Cr (0.03), fayalite for Fe (0.04), diopside for Ca (0.02), and Ni-olivine for Ni (0.05).

[a] Ch = chondrule, G = single mineral grain in matrix.

[b] I = type I FeO-poor chondrule, II = type II FeO-rich chondrule.

[c] Ol = olivine, Ol Rel. = relict grain-bearing olivine, L-Ca Px = low-Ca pyroxene, H-Ca Px = high-Ca pyroxene, and plag = plagioclase.

Table 3
Compositions of opaque minerals (wt.%) in the type I chondrules and matrix of DOM 08006,16.

	Chondrules									Matrix					
Location[a] Op. Type[b]	Ch1 Metal	Ch1 Metal	Ch17 Metal	Ch23 Metal	Ch1 Ni-met	Ch17 Ni-met	Ch23 Ni-met	Ch17 Fe-sulf	Ch17 Fe-sulf	Mx Fe-sulf	Mx Fe-sulf	Mx Ni-met	Mx Ni-met	Mx Metal	Mx Metal
Fe	93.57	90.56	93.36	94.63	40.27	42.09	45.49	62.32	60.03	63.00	63.33	45.12	47.53	91.96	93.47
S	0.04	0.12	bdl	bdl	0.06	0.20	bdl	36.45	36.25	35.66	36.17	34.01	34.08	bdl	bdl
Ni	3.60	6.19	5.30	4.43	55.76	56.94	53.03	0.41	2.65	0.16	bdl	19.67	15.97	6.83	5.12
Co	0.40	0.45	0.40	0.42	1.14	0.58	0.74	0.09	0.19	0.09	0.08	0.18	0.17	0.37	0.40
Cr	0.68	0.95	0.46	0.30	0.14	0.11	0.10	bdl	bdl	bdl	bdl	bdl	bdl	0.59	0.60
Cu	bdl	bdl	bdl	bdl	bdl	bdl	bdl	bdl	bdl	bdl	bdl	0.06	0.29	bdl	bdl
P	0.47	0.29	0.35	0.18	0.47	bdl	bdl	bdl	bdl	bdl	bdl	bdl	bdl	0.42	0.47
Si	0.46	0.33	0.02	bdl	0.48	bdl	bdl	0.04	0.03	bdl	bdl	0.02	0.02	bdl	0.02
Total	0.93	0.62	0.37	0.18	0.96	0.00	0.00	0.04	0.03	0.00	0.00	0.02	0.02	0.42	0.49

bdl = below detection limits.
Standards used for metal and sulfide analyses were Fe-metal for Fe (0.04), pyrite for S (0.03), Ni-metal for Ni (0.5), Co-metal for Co (0.3), Cr-metal for Cr (0.03), Cu-metal for Cu (0.5), galium phosphide for P (0.01), and Si-metal for Si (0.01).
[a] Ch = chondrule, Mx = matrix.
[b] Fe-sulf = iron sulfide, metal = Ni-poor metal, and Ni-met = Ni-rich metal.

A re-extraction step for both samples at slightly elevated temperature (~1750 °C) proved complete degassing of the samples in the main step, apart from a small Ar contribution in the IOM re-extraction, amounting to 1.6 % of the total Ar.

3. RESULTS

3.1. Chromium content of ferroan olivine

All five CO3 chondrites analyzed here contain ferroan olivine in chondrules and as isolated grains in the matrix, which are likely chondrule fragments. Following the procedures of Grossman and Brearley (2005), we analyzed the Cr_2O_3 contents in the cores of 51–60 different ferroan olivine grains within FeO-rich chondrules (i.e., type II; dominated by olivine with Fe/[Fe + Mg] > 10 at.%) and in the matrix from each of the five chondrites in order determine their relative petrographic subtypes (Table 1; Electronic Annex). The resultant data cover a wide range of Cr_2O_3 (wt.%) contents (Fig. 1) that is comparable to the data that have previously been published for the CO3 chondrites (Grossman and Brearley, 2005; Grossman and Rubin, 2006). Four of the CO3 chondrites (DOM 10104, MIL 05024, MIL 090010, and MIL 090470) lie along an apparent trend line between the previously studied primitive CO3s Yamato (Y-) 81020 and Colony, and the more metamorphosed CO3s Kainsaz and Rainbow (Grossman and Brearley, 2005). DOM 08006 plots at a slightly lower mean Cr_2O_3 content and σ-Cr_2O_3 (standard deviation) than the very primitive CO3.03 chondrite ALH 77307 (petrographic subtype determined by Raman spectroscopy of IOM, Bonal et al., 2007, and Fe,

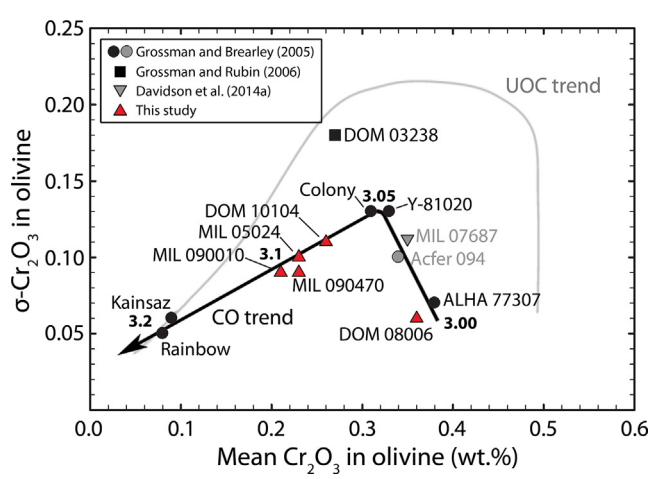

Fig. 1. Plot of the standard deviation (σ) versus the mean of the Cr_2O_3 content (weight percent) of ferroan olivine in CO3 chondrites, including DOM 08006, and ungrouped chondrites Acfer 094 and MIL 07687. A trend line for the CO3 chondrites is shown, along with the ordinary chondrite line from Grossman and Brearley (2005) for comparison. Approximate positions for petrologic subtypes are also shown. Additional data from Grossman and Brearley (2005) and Grossman and Rubin (2006).

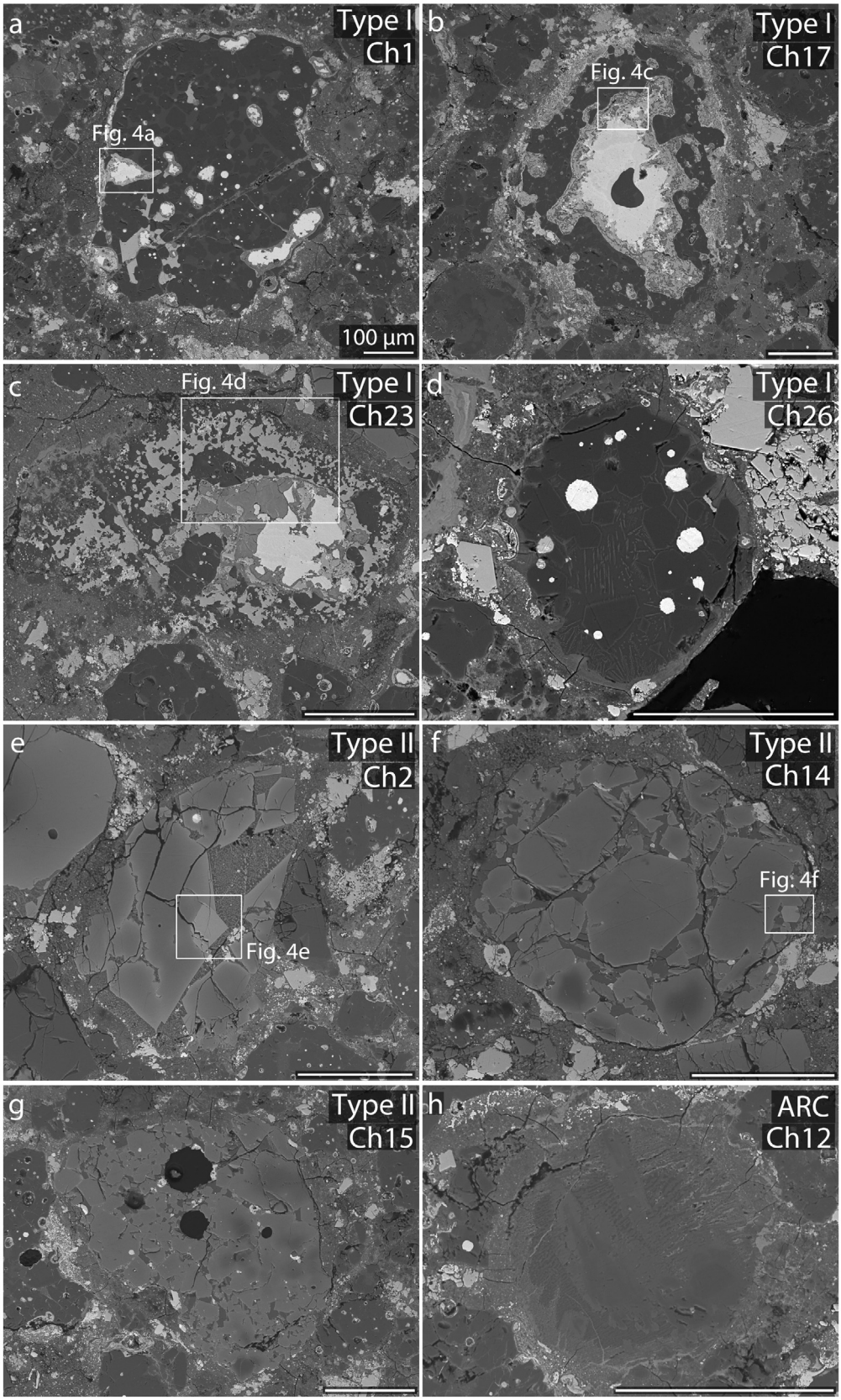

Fig. 2. BSE images of representative chondrules in DOM 08006,16 (a–d) FeO-poor chondrules, (e–g) relict-grain bearing FeO-rich chondrules, and (h) an aluminum-rich chondrule (ARC). All scale bars are 100 µm. See Supp. Fig. 1b for location of chondrules within thin section. Locations of opaque phases in Fig. 4 are marked.

Ni-metal compositions, Kimura et al., 2008), indicating that it may be even more primitive than ALH 77307.

3.2. Petrography of DOM 08006

3.2.1. General description and modal mineralogy

DOM 08006 contains abundant chondrules, chondrule fragments, and mineral grains in an optically dark matrix. The thin section studied here (total sample area of 72 mm^2) consists of 90 vol.% silicate and 10 vol.% opaque minerals, similar to the modal mineralogy of DOM 08006 determined via PSD-XRD (Alexander et al., 2018). Silicate phases consist of ~67 vol.% chondrules, 22 vol.% matrix, and ~1 vol.% refractory inclusions (Ca-, Al-rich inclusions [CAIs] and Amoeboid Olivine Aggregates [AOAs]). The ~67 vol.% chondrules consist of 49 vol.% FeO-poor (i.e., type I; dominated by olivine with Fe/[Fe + Mg] < 10 at. %), 17 vol.% FeO-rich, and <1 vol.% Al-rich chondrules. The chondrule/matrix volume ratio is ~3. Opaque phases are primarily metal (~1.9 vol.%), sulfide (1.0 vol.%), chrome-spinel (≪0.5 vol.%), and magnetite and terrestrial weathering products (<7.1 vol.%). It was not possible to distinguish terrestrial weathering products (mostly amorphous Fe-oxide-hydroxide) from presumably parent body-formed magnetite in large area BSE maps (e.g., Suppl. Fig. 1). Since terrestrial weathering likely affected not just magnetite, but multiple phases such as metal and sulfide, it is not appropriate to assume all terrestrially weathered material was once magnetite; the true magnetite abundance is likely to be lower. No phyllosilicates were observed.

3.2.2. Chondrule textural types and silicate mineralogy

Apparent chondrule diameters range from ~50 μm to 620 μm, with an average of 133 ± 85 μm (mean ± 1SD; n = 317), which is similar to the 150 μm average reported for the CO chondrites (e.g., Rubin, 1989, 2000, 2010; Scott and Krot, 2005). The most dominant chondrule textural types are porphyritic-olivine-pyroxene (POP) and porphyritic-olivine (PO) chondrules (Fig. 2a–g; Table 4). FeO-poor chondrules (~73 vol.% of all chondrules; Fig. 2a–d) are much more abundant than FeO-rich chondrules (~25 vol.%; Fig. 2e–g) and Al-rich chondrules (<2 vol.% Fig. 2h). Compound chondrules are rare, although in one instance a small (<50 μm diameter) Al-rich chondrule was completely enveloped by a FeO-poor POP chondrule.

FeO-poor chondrules (Fig. 2a–d) consist of predominantly forsteritic olivine ($Fa_{0–1}$) (Supp. Fig. 3), with minor amounts of low-Ca ($En_{96–99}Fs_{1–2}Wo_{1–3}$) and high-Ca pyroxene ($Wo_{15–45}$). Both dusty olivine and dusty pyroxene are present in FeO-poor chondrules (Fig. 3e, g). FeO-rich chondrules (Fig. 2e–g) are predominantly olivine ($Fa_{12–45}$; Supp. Fig. 3), and contain FeO-poor relict grains ($Fa_{3–6}$), and minor amounts of both low-Ca ($En_{98}Fs_1Wo_1$) and high-Ca ($En_{42–61}Fs_{11–14}Wo_{28–43}$) pyroxene.

Small amounts of compositional zoning were observed in chondrule silicates (Supp. Fig. 4). Isolated fayalite-rich olivine grains in the matrix exhibit increases in FeO, MnO, and CaO at the grain rims, which is common in FeO-rich chondrules in ALH 77307 (Jones, 1992) and other CO3 chondrites (Scott and Jones, 1990). Chromium contents (reported as Cr_2O_3) also increase towards the grain edges but decrease at the outermost part of the rims, which is also commonly seen in FeO-rich chondrules (e.g., Jones, 1992). Aluminum contents (Al_2O_3) are very low, in some cases below detection limits.

3.2.3. Plagioclase compositions

Plagioclase was analyzed in 11 chondrules (10 FeO-poor, one FeO-rich) from DOM 08006 and has compositions of $An_{68–99}$ (Table 2). The excess silica molar fraction, $[\ ]Si_4O_8$, within chondrule plagioclase was calculated per the method of Beaty and Albee (1980) using the following formulae:

$$Ca(Fe,Mg)Si_3O_8 = 4 - (Si + Al) \quad (1)$$

$$[\ ]Si_4O_8 = 1 - [Na + Mg + K + Ca + Fe + Ba - Ca(Fe,Mg)Si_3O_8] \quad (2)$$

Calculated excess silica abundances range from −1.8 mol.% to 6.9 mol.%; the plagioclase in five chondrules (all FeO-poor) show resolvable excesses in silica.

Table 4
Modal abundances and average olivine and low Ca pyroxene compositions of individual chondrules within DOM 08006,16.

Chondrule number	Type[a]	Texture[b]	Olivine		Low Ca pyroxene						Modal abundances[c]							
			Fa		En		Fs		Wo		Ol	Px	Plag/ Meso[d]	Met	Sulf	Mag	Chr	TW
1	I	POP	1.0	(0.1)	97.8	(0.8)	1.3	(0.6)	0.9	(0.2)	39.8	10.0	27.7	6.6	1.3	6.1	0.0	8.6
2	II	PO	32.1	(8.0)							55.5	0.0	36.9	0.2	1.9	0.0	5.5	0.0
5	I	POP	0.9	(0.1)	98.4	(0.3)	0.7	(0.1)	1.0	(0.2)	13.4	45.7	22.4	0.3	0.8	6.3	0.0	11.1
14	II*	PO	33.7	(6.8)							75.1	0.0	16.1	0.0	3.7	0.0	5.1	0.0
15	II*	PO	27.9	(13.1)							82.6	0.0	12.8	0.0	1.2	1.0	2.5	0.0
17	I	PP			96.8	(0.4)	2.0	(0.4)	1.1	(0.1)	0.0	28.0	9.6	18.1	4.0	24.7	0.0	15.6
23	I	POP	28.9	(4.5)							44.8	5.0	0.0	8.7	0.8	24.7	0.0	16.1

[a] I = type I FeO-poor chondrule, II = type II FeO-rich chondrule. *indicates chondrule contains relict-grains.
[b] PO = porphyritic olivine; PP = porphyritic pyroxene; POP = porphyritic olivine pyroxene.
[c] Ol = olivine, Px = Pyroxene, Plag = plagioclase, Meso = mesostasis, Met = metal, Mag = magnetite, Chr = chrome-spinel, TW = terrestrial weathering products.
[d] It was not possible to distinguish between plagioclase and mesostasis in BSE images thus the reported abundances combine the two phases.

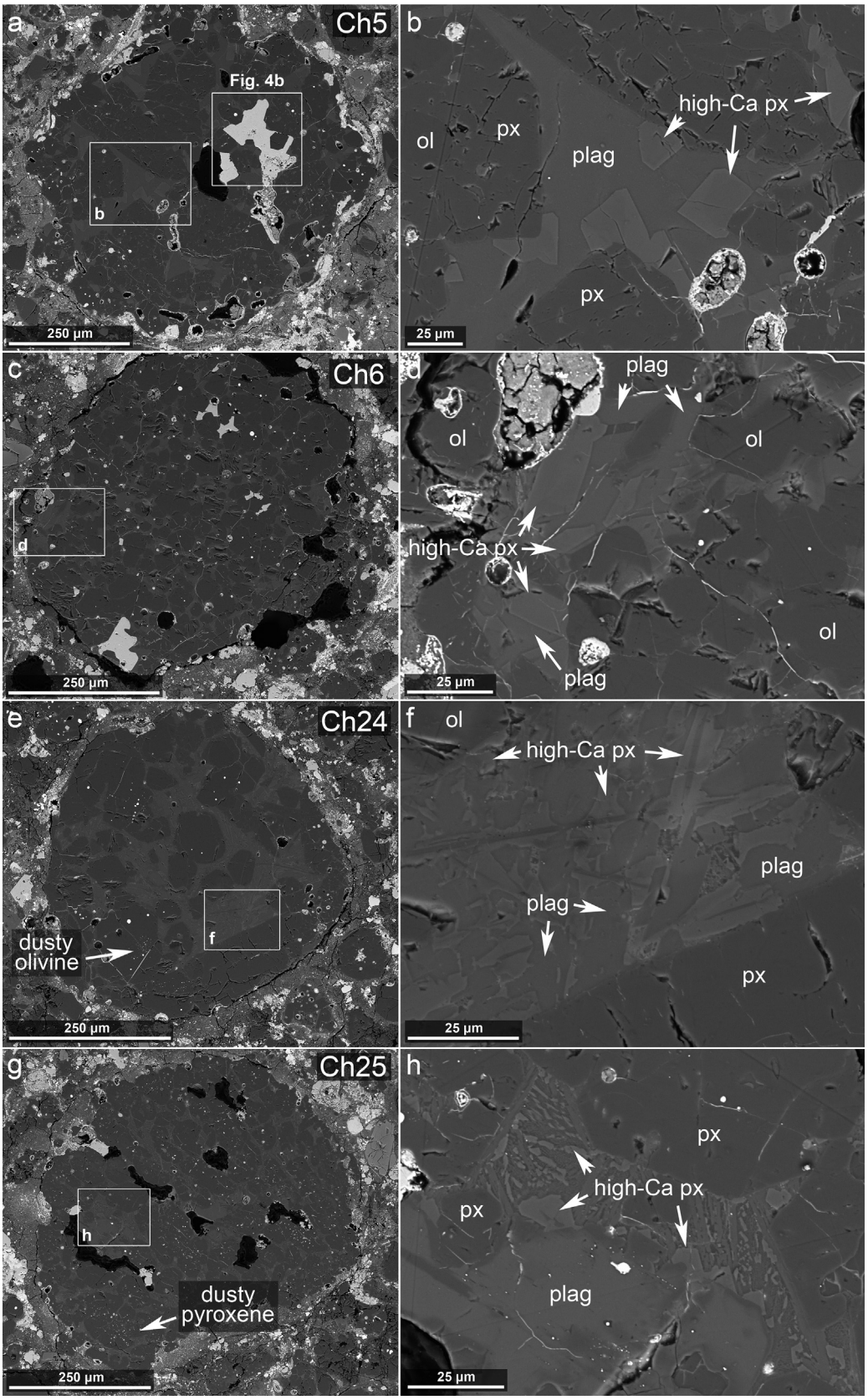

Fig. 3. BSE images of (a,c,e,g) FeO-poor chondrules and (b,d,f,h) their plagioclase textures. (e,f) Chondrule 24 contains dusty olivine. (g,h) Chondrule 25 contains dusty pyroxene.

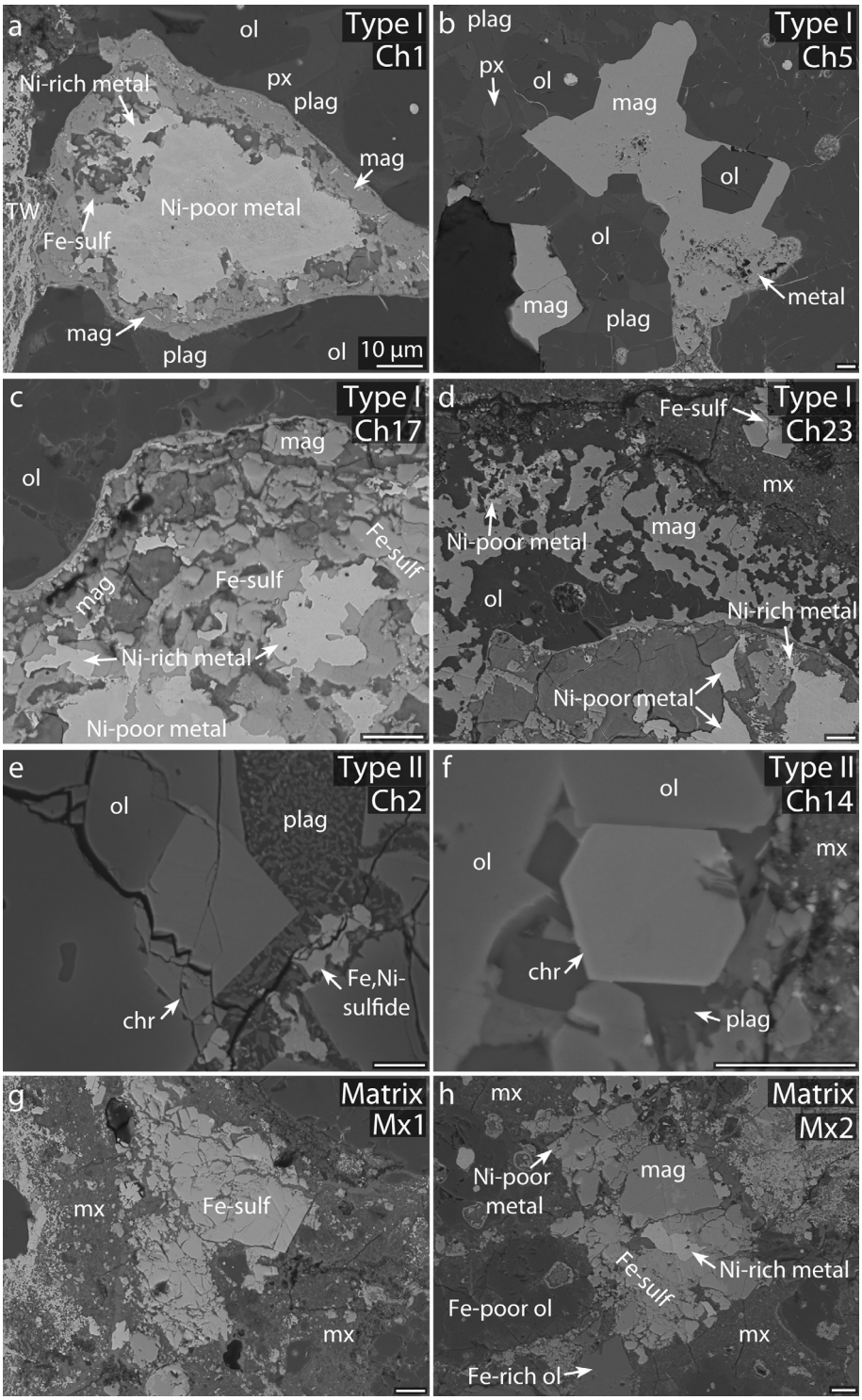

Fig. 4. BSE images of representative opaque assemblages in (a–d) FeO-poor and (e,f) FeO-rich chondrules, and (g,h) matrix in DOM 08006,16. (a) Metal-sulfide assemblage that has been partially oxidized to magnetite in chondrule 1 (FeO-poor), (b) magnetite surrounding individual olivine and pyroxene crystals contains trace amounts of remaining metal in chondrule 5 (c) part of a large opaque mineral assemblage from the interior of chondrule 17 containing both Ni-rich and Ni–poor metal, Fe-sulfide and magnetite, (d) part of the extremely opaque-rich chondrule 23, which contains Fe,Ni-metal in the chondrule interior and magnetite at the chondrule rims, (e) a euhedral chrome-spinel grain and Fe,Ni-sulfide (rare in FeO-rich chondrules) in chondrule 2, (f) a euhedral chrome-spinel grain in chondrule 14, (g) large Fe-sulfide in matrix (Mx1), and (h) a large opaque assemblage of primarily Fe-sulfide and magnetite with minor amounts of Ni-rich and Ni-poor metal in matrix (Mx2). See Supp. Fig. 1b for location within thin section and Fig. 2 for locations within chondrules. Where; chr = chrome-spinel, Fe-sulf = iron sulfide, mag = magnetite, mx = matrix, ol = olivine, plag = plagioclase, and px = pyroxene, TW = terrestrial weathering products. See Supp. Fig. 2b for locations of opaque-rich chondrules and OAs in matrix in the thin section.

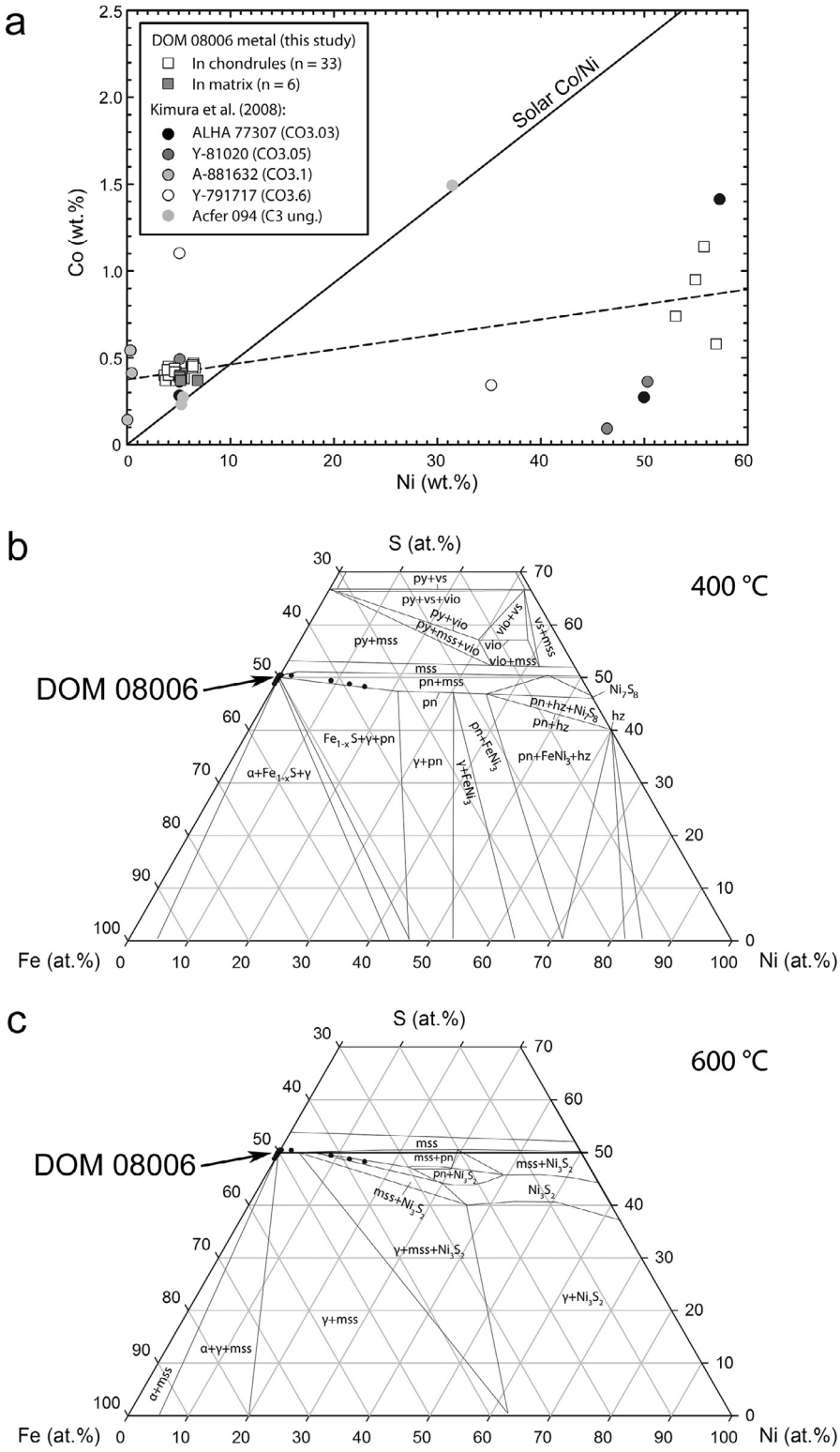

Fig. 5. (a) Cobalt and nickel (both weight percent) content of individual metal grains in chondrules and matrix of DOM 08006,16. Average compositions of kamacite and Ni-rich metal from CO chondrites and the ungrouped chondrite Acfer 094 are shown for comparison (Kimura et al., 2008). The solar Co/Ni ratio line (data from Lodders et al., 2009) is shown for comparison to the line of slope for DOM 08006 metal data: Co (wt.%) = (0.0087 ± 0.0016) × Ni (wt.%) + (0.3753 ± 0.0336), where the correlation coefficient R = 0.8776. (b, c) Sulfide data from opaque assemblages in chondrules and matrix of DOM 08006,16 are shown on Fe-Ni-S isothermal phase diagrams at (b) 400 °C and (c) 600 °C. Adapted from Schrader et al. (2015) after Raghavan (2004), original data from (b) Craig et al. (1968) and (c) Kozyakov et al. (2003). Where α = kamacite, γ = taenite, pn = pentlandite, py = pyrrhotite, hz = heazlewoodite (Ni_3S_2), vs = vaesite (NiS_2), vio = violarite (Ni_3S_4).

3.2.4. Opaque mineral assemblages

Opaque mineral assemblages (OAs) are found along chondrule exteriors, within chondrule interiors, and in the matrix of DOM 08006 (see Fig. 2 for the distribution of OAs associated with chondrules; see Supp. Fig. 2b for the distribution of Fe, Ni, and S throughout the thin section). Opaque minerals associated with FeO-poor and FeO-rich chondrules typically consist of abundant magnetite and metal (including Ni-poor kamacite and Ni-rich taenite). Aluminum-rich chondrules generally lack opaque minerals. The sulfide minerals present in chondrules and matrix were troilite (FeS; atomic ratios of Fe/S = ~1.00), pyrrhotite ($Fe_{(1-X)}S$; Fe/S from 0.98–1.01), and Ni-rich pyrrhotite (Ni up to 11.6 wt.%; Fe/S = 0.85–0.95). Pentlandite ([Fe, Ni]$_9S_8$; 16–20 wt.% Ni, Fe/S = variable) was only observed in the matrix. Modal abundances were calculated for a number of representative chondrules (Table 4); opaque abundances are lower limits as the chondrules have been terrestrially weathered to different degrees (opaque phases weather more rapidly than silicates).

FeO-poor chondrules contain from ~8 vol.% to 47 vol.% OAs, including approximately 0.3–18.1 vol.% metal, 6.1–24.7 vol.% magnetite, and 0.8–4.0 vol.% sulfide (Table 4). When present in FeO-poor chondrules, sulfides are located in the outermost portions of the chondrule and along the exterior rim. Sulfide grains are generally smaller in chondrules than in matrix (Fig. 4). Both Ni-poor (≤7 wt.% Ni; kamacite) and Ni-rich (20–50 wt.% Ni; taenite) metal are present in chondrules (Fig. 5). Nickel-poor metal contains 90.6–95.6 wt.% Fe, 3.6–6.8 wt.% Ni, and 0.37–0.47 wt.% Co (Table 3). Nickel-rich metal contains 40.3–45.5 wt.% Fe, 53.0–56.9 wt.% Ni, and 0.58–1.14 wt.% Co (Table 3).

Although very rare, sulfides are located throughout FeO-rich chondrules, in contrast to FeO-poor chondrules where sulfides are only found closer to the chondrule rim than core. However, FeO-rich chondrules are generally much smaller in diameter than larger FeO-poor chondrules and the distance from the chondrule rims to sulfide minerals is consistent between both chondrule types. FeO-rich chondrules contain between ~5 vol.% and 9 vol.% opaque minerals (Fig. 2e–g; Table 4), which primarily consist of chrome-spinel (2.5–5.5 vol.%) and sulfide (≤3.7 vol.%), and only very minor amounts of metal (≤0.2 vol.%) and magnetite (≤1 vol.%). Chrome-spinel grains are located exclusively in FeO-rich chondrules; they are generally very euhedral (Figs. 2e,f and 4e,f), and internally homogeneous with an average Cr_2O_3 content of ~47 wt.%, FeO of ~27 wt.%, and Fe_2O_3 of ~3 wt.%. Not all FeO-rich chondrules appear to be chrome-spinel-bearing – although this may be a thin sectioning artefact.

Magnetite in DOM 08006 is present in both FeO-poor and FeO-rich chondrules. Magnetite is most abundant in

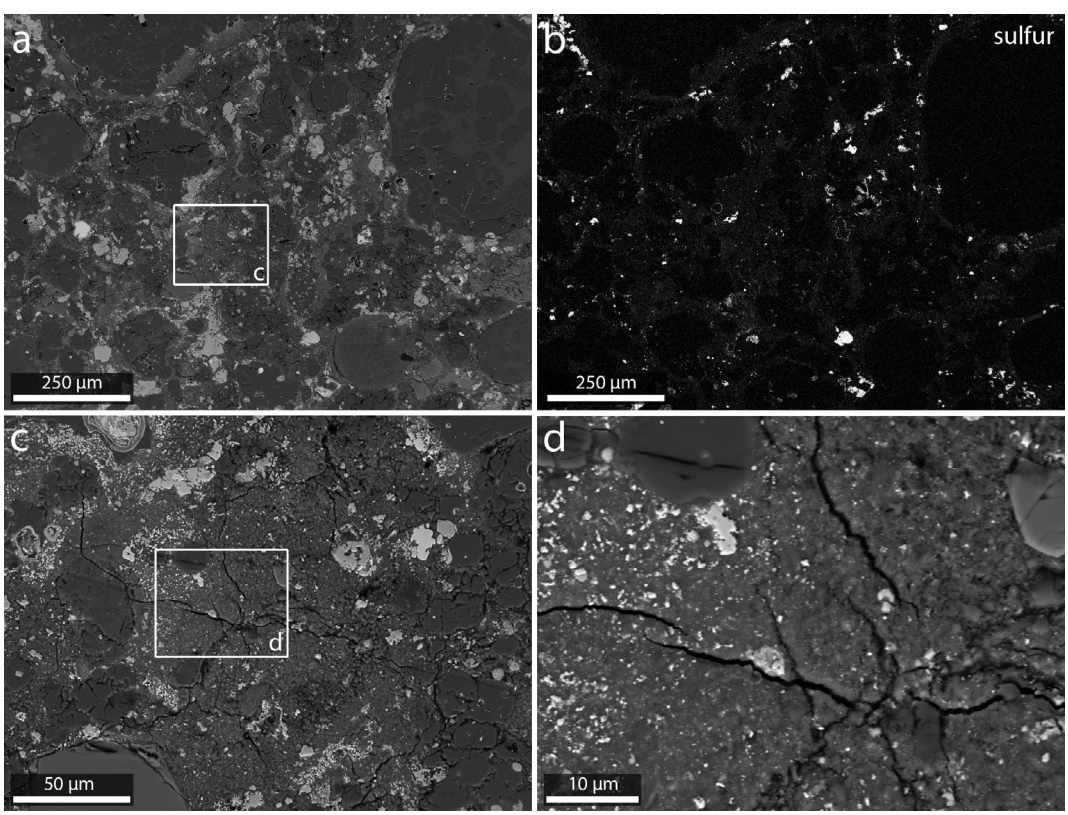

Fig. 6. Various images showing an area of characteristic matrix in DOM 08006,16. (a, c, d) BSE images of the same area at different scales where the brightest phases represent opaque minerals (such as metal, magnetite and sulfide), (b) an elemental X-ray map showing the distribution of sulfur across the same area of matrix and at the same scale as (a) demonstrating the widespread nature of S in the matrix indicating that the sample is not significantly altered, (d) many sub-500 nm sulfide grains are present.

FeO-poor chondrules (up to 24.7 vol.%; Table 4), and while some magnetite is found at chondrule exteriors, the majority is found rimming Fe,Ni-metal grains within the chondrule interiors (Figs. 2a–c, 4a–d). Magnetite is much less abundant in FeO-rich chondrules (≤1 vol.%; Table 4), and is most often located at the outer edges of the chondrules (Fig. 2f). Magnetite occurs as either intergrowths with Fe,Ni-metal (both Ni-rich and Ni-poor) and Fe-sulfide that surround larger Fe,Ni-metal grains (Fig. 4a,c), or as almost entirely uniform and infilled space between silicate grains (Fig. 4b,d). Terrestrial weathering experienced by DOM 08006 has led to the destruction of some magnetite grains (Fig. 4a,c), while others remain mostly intact (Fig. 4b).

Magnetite is compositionally the same in both FeO-poor and FeO-rich chondrules, being composed predominantly of Fe (FeO: 30.1–30.5 wt.%; Fe_2O_3 = 67.2–67.9 wt.%), and containing minor amounts of Al_2O_3 (≤0.02 wt.%), MgO (≤0.03 wt.%), CaO (≤0.07 wt.%), and Cr_2O_3 (≤0.12 wt.%), while Na_2O, SiO_2, NiO, MnO, and TiO_2 were all below detection limits. The magnetite grains in the most terrestrially weathered regions were too small from which to obtain compositional analyses.

3.2.5. Matrix

The matrix consists of fine-grained silicate, metal, magnetite and abundant sulfide minerals. Where present, Fe,Ni-metal is typically kamacite and contains 92.0–93.9 wt.% Fe, 5.1–6.8 wt.% Ni, and 0.37–0.40 wt.% Co. Small amounts of taenite metal were observed, but were too small for analysis. Magnetite–metal assemblages may be up to ~400 μm in diameter (see Supp. Fig. 2b). Fine-grained (submicron) sulfides are present throughout the matrix of DOM 08006 (Fig. 6), similar to ALH 77307 (Grossman and Brearley, 2005), but can also reach up to ~150 μm in diameter (e.g., Mx1; Fig. 4g). Sulfides are sometimes associated with metal (e.g., Mx2; Fig. 4h).

Olivine grains in the matrix are likely chondrule fragments, but are generally more ferroan (up to Fa_{71}) than intact chondrules ($Fa_{<45}$) (Supp. Fig. 3), and are also commonly zoned (e.g., ~Fa_{42} to Fa_{67}; core to rim). Low-Ca pyroxene within the matrix is generally Fe-rich ($En_{52-60}Fs_{39-46}Wo_1$). High-Ca pyroxene within the matrix is also Fe-rich ($En_{32}Fs_{50}Wo_{18}$; 1 analysis).

TEM analyses (Figs. 7 and 8, and Suppl. Figs. 5 and 6) of five FIB sections of the finest grained matrix revealed that it contains highly unequilibrated mixtures of amorphous Fe-rich silicate, olivine (<200 nm diameter), pyroxene (mostly < 500 nm diameter), metal, sulfides and organic carbon. No clastic grains were identified. The organic carbon appears as distinct (50 nm to 500 nm diameter) blebs, and in veins. The sulfide minerals (10 nm to 200 nm diameter) present include both pyrrhotite and pentlandite. The polycrystalline appearances and intermediate Ni contents (Ni/Fe ~ 0.3) of many pentlandite grains indicate that they may be intergrowths of metal and sulfide. Some large polycrystalline pyroxene grains (~1 μm diameter) contain small chrome-spinel sub-grains (~5 nm; Fig. 8). No Fe-rich rims were observed on Mg-rich olivine grains or amorphous silicate minerals either by dark-field STEM imaging or EDS mapping (Suppl. Figs. 5 and 6). No phyllosilicates were detected in the amorphous material either by selected area diffraction or HRTEM imaging. Needles of Fe oxy-hydride were observed in one FIB section, consistent with DOM 08006 having experienced some terrestrial weathering (Fig. 7b). However, as DOM 08006 exhibits

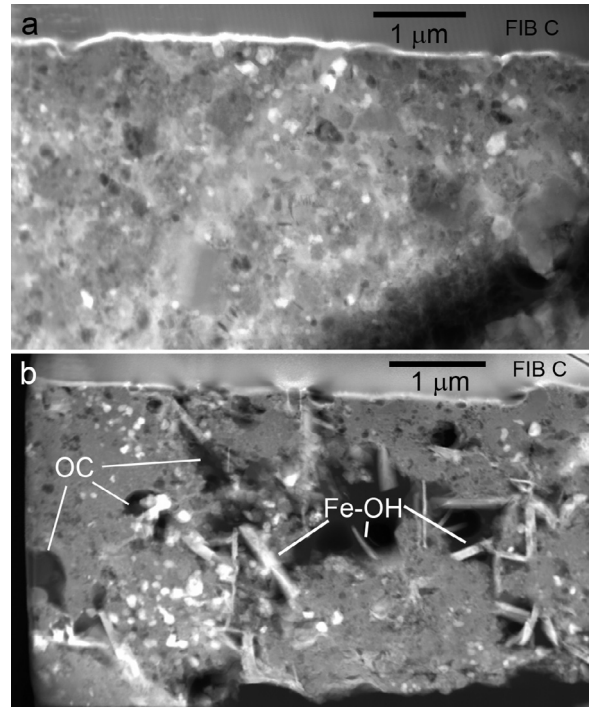

Fig. 7. HAADF scanning transmission electron microscopy images of two extracted electron-transparent sections from the fine-grained matrix of DOM 08006. (a) The matrix is dominated by grains < 100 nm diameter, including crystalline and amorphous silicates, sulfides, metal and organic carbon (OC). Carbon-rich veins are also present. (b) Needles of Fe oxy-hydride (Fe-OH) are present in one section, suggestive of terrestrial weathering.

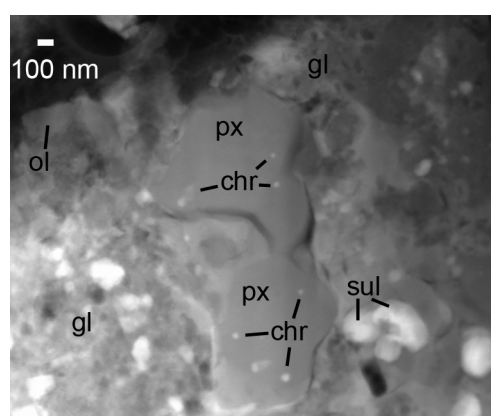

Fig. 8. HAADF scanning transmission electron microscopy image. Isolated 100-nm scale olivine (ol) and glass (gl) regions are preserved, but two rounded pyroxenes (px) contain sub-grains of chrome-spinel (chr) consistent with initial stages of thermal mobilization of Cr. Where ol = olivine, and sul = sulfide.

evidence for having undergone minor amounts of parent body aqueous alteration, the possibility that some hydroxides formed in the CO parent body cannot be eliminated. Each of the FIB sections was positioned to contain one or more O-rich presolar grain. These grains, include two Mg-rich olivines, one amorphous grain with a pyroxene-like composition, and one zoned grain with a silicate shell surrounding an oxide core. All the presolar grains were well preserved, with no detectable signs of thermal metamorphism or aqueous alteration. Additional details about the analyzed presolar grains can be found in Nittler et al. (2018).

3.2.6. Refractory inclusions

Refractory inclusions (CAIs and AOAs) account for only ~1 vol.% of the total DOM 08006 thin section studied herein. The CAIs in DOM 08006 are generally small (<100 μm in diameter). However, several larger CAIs (up to 430 μm in diameter) are also present. The mineral assemblages present in DOM 08006 CAIs commonly possess rims of melilite and Al-diopside. As such, they are similar to CAIs seen in Acfer 094 (Simon and Grossman, 2011). The mineralogies of CAIs from DOM 08006 have been discussed in detail by Simon and Grossman (2015) and are not considered further here. AOAs are rare in DOM 08006; only one was seen in this study (≪0.1 vol.% of total thin section) and was of similar size to the smaller CAIs (~90 μm in diameter). An AOA surrounded by a ferroan igneous rim was observed in a different thin section (DOM 08006,39; Nagashima et al., 2015); the AOA identified in this study did not possess an igneous rim.

3.3. Noble gases

Noble gas analysis (Tables 5–7) of the bulk DOM 08006 sample yielded the expected mixture of trapped, cosmogenic and radiogenic noble gas components, while DOM 08006 IOM contains exclusively trapped noble gases as anticipated. The reader is directed to Ott (2014) for a detailed breakdown of the different planetary and presolar noble gas components found in meteorites. Neon in the bulk sample shows a significant contribution from cosmogenic Ne, enabling the determination of cosmogenic ^{21}Ne (Table 5) by two-component deconvolution. Extrapolating from IOM-Ne through bulk Ne to the canonical $(^{20}Ne/^{22}Ne)_{cosm}$ range from 0.7 to 0.9 yields a $(^{21}Ne/^{22}Ne)_{cosm}$ ratio between 0.948 and 0.978. Such high ratios are rather unlikely (cf. discussion by Bartoschewitz et al., 2010). The Leya and Masarik (2009) model for cosmogenic nuclides combined with average CO chondrite chemistry (Lodders and Fegley, 1998) would imply very large shielding and, in view of the recovered mass of 0.7 kg, a rather unlikely pre-atmospheric radius of ≥120 cm (and 25 ton mass) for these $(^{21}Ne/^{22}Ne)_{cosm}$ ratios.

However, bulk DOM 08006 may also contain other trapped Ne components that are no longer present in the IOM after demineralization, such as solar wind Ne or one of the components with ^{20}Ne/^{22}Ne well above that of Ne-HL but distinct from air that has recently been found to be abundant in a primitive CR chondrite (Krietsch et al., 2019). If one of these components is present in the IOM, the IOM-Ne composition cannot be used as a trapped end-member. Instead, although there is no evidence for solar

Table 5
Helium and Ne concentrations (in 10^{-8} cm^3 STP/g) and isotopic ratios in a bulk and IOM sample of DOM 08006.

	$^3He_{(cos)}$	^{4}He	^{3}He/^{4}He × 10,000	^{20}Ne	^{20}Ne/^{22}Ne	^{21}Ne/^{22}Ne	$^{21}Ne_{cos}$	$^4He_{rad}$
Bulk	28.74 ± 0.17	2167 ± 16	132.6 ± 1.3	26.82 ± 0.19	2.877 ± 0.010	0.6917 ± 0.0021	6.28 ± 0.10	2005 ± 21
IOM	n.d.	1722 ± 18	153 ± 15	26.43 ± 0.15	0.82 ± 0.03	0.90 ± 0.04	n.d.	n.d.

n.d. = not detectable.

Table 6
Argon and Kr concentrations (in 10^{-8} and 10^{-10} cm^3 STP/g respectively) and isotopic ratios in a bulk and IOM sample of DOM 08006.

	^{36}Ar	^{36}Ar/^{38}Ar	^{40}Ar/^{36}Ar	^{84}Kr	^{78}Kr/^{84}Kr	^{80}Kr/^{84}Kr	^{82}Kr/^{84}Kr (^{84}Kr = 100)	^{83}Kr/^{84}Kr	^{86}Kr/^{84}Kr
Bulk	285.1 ± 8.6	5.342 ± 0.027	0.76 ± 0.11	134.1 ± 1.9	0.513 ± 0.022*	3.98 ± 0.11	20.19 ± 0.34	20.27 ± 0.30	30.48 ± 0.50
IOM	1307 ± 43	5.349 ± 0.018	0.72 ± 0.28	1770 ± 30	0.579 ± 0.006	3.868 ± 0.032	19.95 ± 0.16	19.84 ± 0.18	30.93 ± 0.21

* Probably too low due to peak centring problems.

Table 7
Xenon concentrations (in 10^{-10} cm^3 STP/g) and isotopic ratios in a bulk and IOM sample of DOM 08006.

	^{132}Xe	^{124}Xe/^{132}Xe	^{126}Xe/^{132}Xe	^{128}Xe/^{132}Xe	^{129}Xe/^{132}Xe (^{132}Xe = 100)	^{130}Xe/^{132}Xe	^{131}Xe/^{132}Xe	^{134}Xe/^{132}Xe	^{136}Xe/^{132}Xe
Bulk	156.5 ± 4.1	0.429 ± 0.011	0.3941 ± 0.0075	7.89 ± 0.10	104.80 ± 1.33	15.94 ± 0.16	82.25 ± 0.80	39.05 ± 0.45	32.99 ± 0.39
IOM	4328 ± 129	0.3961 ± 0.0052	0.3646 ± 0.0036	7.453 ± 0.055	99.10 ± 1.14	15.38 ± 0.11	79.78 ± 0.58	38.07 ± 0.29	32.34 ± 0.25

wind in DOM 08006, somewhat conservatively using typical meteoritic SW-Ne with $^{20}Ne/^{22}Ne = 12.5 \pm 0.1$ and extrapolating through the DOM 08006 data point, yields $(^{21}Ne/^{22}Ne)_{cosm}$ in the range 0.825 to 0.841. Fundamentally, $(^{21}Ne/^{22}Ne)_{cosm}$ cannot be sufficiently constrained to obtain reliable shielding conditions and, hence, a cosmic ray exposure age with Leya and Masarik's model. The $^{3}He/^{4}He$ ratio of bulk DOM 08006 is $(132.6 \pm 1.3) \times 10^{-4}$, suggesting that the measured ^{3}He is almost entirely cosmogenic, with $(^{3}He/^{4}He)_{cosm} \sim 0.2$.

For the sake of comparability, using the "adopted average" shielding ratio $(^{21}Ne/^{22}Ne)_{cosm} = 0.901$ and the formulas given by Eugster (1988) that were both used by Scherer and Schultz (2000), a cosmic ray exposure age of DOM 08006 is calculated to be ~20 Ma from ^{3}He and 18 Ma from ^{21}Ne. Typically, uncertainties of 15–20% can be adopted for such a calculation of exposure gases based on noble gases.

Neon in DOM 08006 IOM is consistent with a mixture of Ne-HL, residing in presolar diamonds (Huss and Lewis, 1994), and a small addition of Ne-E (now also Ne-R and Ne-G), residing in presolar graphite and SiC (Lewis et al., 1994, Amari et al., 1995). The IOM has a $^{3}He/^{4}He$ of $(1.68 \pm 0.04) \times 10^{-4}$ (i.e., its He consists mainly of He-HL; Huss and Lewis, 1994). Argon in both the bulk and IOM samples isotopically resembles pure Ar-Q (Busemann et al., 2000) and, hence, $^{38}Ar_{cosm}$ in the bulk cannot be determined. Krypton and Xe isotopes in bulk DOM 08006 are similar to Q-Kr and Q-Xe (Busemann et al., 2000), perhaps with a small addition of Xe-HL that is detectable in the heaviest Xe isotopes. The Xe isotopes of the IOM show large contamination with air Xe (~2/3 of the total Xe, based on the required mixing ratios between Q-Xe and air-Xe). Hence, we cannot use the elemental ratios $^{36}Ar/^{132}Xe$ and $^{84}Kr/^{132}Xe$ of the IOM for comparison with published literature. These ratios could be used to assess the degree of alteration experienced in the parent body (cf. Busemann et al., 2000). However, the bulk sample was much less affected by terrestrial Xe contamination based on the Xe isotopes. The $^{36}Ar/^{132}Xe$ ratio of 195 $\pm$ 20 suggests the presence of an Ar-rich component, that is similar to what has been found in the bulk analyses of many primitive chondrites (e.g., Mazor et al., 1970; Alaerts et al., 1979a, 1979b; Matsuda et al., 1980).

4. DISCUSSION

4.1. A CO metamorphic sequence

Grossman and Brearley (2005) have shown that, for the least altered unequilibrated ordinary and CO chondrites, the Cr-contents (reported as Cr_2O_3) of ferroan olivines evolved during thermal metamorphism and can be used to identify the most minimally thermally metamorphosed samples. Before the onset of thermal metamorphism, the initial Cr-content of olivine is high and relatively homogeneous (reflected by high mean Cr_2O_3 abundances and a low standard deviation: σ-Cr_2O_3; Fig. 1). As the earliest stages of metamorphism progress, chromite exsolves from olivine, lowering the Cr-content of olivine grain cores and creating heterogeneity (lower mean Cr_2O_3 abundances and higher σ-Cr_2O_3; Fig. 1). Further metamorphism drives diffusion of Cr out of the olivine grains, ultimately resulting in homogeneously low Cr-contents of the olivine cores and enrichment at the grain boundaries/rims (low mean Cr_2O_3 and low σ-Cr_2O_3; Fig. 1; Grossman and Brearley, 2005). As such, the mean Cr abundances of ferroan olivines (from ~50 individual grain cores) and their standard deviations in primitive samples can be used as a comparative way of determining their metamorphic subtypes.

This scheme was originally calibrated for the unequilibrated ordinary chondrites (UOCs) and, to a lesser extent, the CO chondrites (Grossman and Brearley, 2005). The trend for the CO chondrites was not well-defined and the suggestion that magnetite-rich DOM 03238 may represent the so-called "missing link" between petrologic type ~CO3.1 (Colony/Y-81020) and ~CO3.2 (Rainbow/Kainsaz) chondrites, and thus define the metamorphic trend (Grossman and Rubin, 2006), was later refuted (see Davidson et al., 2014b and data presented here). Since the initial Cr-contents of ferroan olivine may differ between chondrite groups (e.g., Davidson et al., 2015; Davidson et al., 2019; Schrader et al., 2015; Schrader and Davidson, 2017), it is not appropriate to compare these parameters between chondrite groups. Furthermore, the exsolution of Cr is a diffusive process that depends upon thermal history, i.e., type of heating (radiogenic or impact-driven), duration of heating, and peak temperature. Thus, this scheme should only be used to internally compare within chondrite groups and not between those that have been subjected to drastically different parent body conditions.

Following the procedures of Grossman and Brearley (2005), we analyzed the Cr-contents of the centers of between 51 and 60 different ferroan olivine grains within FeO-rich chondrules and chondrule fragments in each of the five CO chondrites of this study (Table 1; Section 3.1). On the basis of mean Cr-content versus standard deviation in ferroan olivine (Fig. 1), DOM 08006 appears to be as primitive as, if not more primitive than, ALH 77307 (CO3.03). The four other CO3s analyzed here are of higher petrographic grade, lying along an apparent trend somewhere between Colony (CO3.05) and Kainsaz and Rainbow (CO3.2). Although a Raman spectroscopic study of IOM within Kainsaz indicates that this sample may be of higher petrologic type CO3.6 (Bonal et al., 2007), this is not reflected by the petrology of this sample (e.g., McSween, 1977). Thus, we choose to use a subtype of CO3.2 for Kainsaz based on petrographic observations. When combined with data from previous studies, the Cr_2O_3 compositions of ferroan olivine in DOM 10104, MIL 05024, MIL 090470, and MIL 090010 fill in the pre-existing gap between Colony/Y-81020 and Kainsaz/Rainbow. This trend appears to define the CO3.00 to 3.2 metamorphic sequence that can be used to calibrate the comparable CO3 scale to that used for the OCs (Grossman and Brearley, 2005). On this basis, we consider DOM 08006 to be of metamorphic grade CO3.00, and DOM 10104, MIL 05024, MIL 090470, and MIL 090010 to all be CO3.1. This is consistent with the matrix of MIL 090010 appearing to have experienced higher peak metamorphic temperatures than the matrix of DOM 08006 (Bonato et al., 2019). DOM 03238,

which is known to be unusually magnetite-rich (7.6 vol.%), appears to be an outlier (Grossman and Rubin, 2006). The general trend of alteration shown by DOM 03238 (Grossman and Rubin, 2006), DOM 08006, DOM 10104, MIL 05024 and MIL 090010 is consistent with their bulk C abundances (Alexander et al., 2018).

4.2. DOM 08006: A very primitive CO3 chondrite

This section discusses different mineralogical measures for determining how "primitive" DOM 08006 is via the study of: (1) interchondrule matrix, (2) opaque minerals, and (3) silicate minerals. Data are discussed in this sequence as they represent the approximate order of sensitivity to alteration/metamorphism in the parent body.

4.2.1. Interchondrule matrix

While there appears to be no significant parent body aqueous alteration of interchondrule matrix on a scale of 10 μm to 100 μm, some metal has been altered to magnetite, indicating that at least minor amounts of aqueous alteration have taken place (Fig. 6). However, this aqueous alteration was not extensive enough to impact the high concentration in the matrix of preserved presolar silicate grains, which are rapidly destroyed during parent body aqueous alteration (Nittler et al., 2018).

Microscale TEM analysis of interchondrule matrix in DOM 08006 indicates only very minor aqueous alteration, revealing abundant amorphous silicate and sub-100 nm sized grains of metal, sulfide, olivine, and pyroxene (Fig. 7). The similarity between the Cr-content parameters determined for the ferroan olivine from ALH 77307 (CO3.03) and DOM 08006 (suggested CO3.00 here) is supported by comparison of the sub-micron components of the matrices of both chondrites. In fact, the DOM 08006 matrix mineralogy is very similar to those of ALH 77307 (Brearley, 1993; Brunner and Brearley, 2011) and the primitive ungrouped carbonaceous chondrite Acfer 094 (Greshake, 1997); all three are comprised of similar-sized, unequilibrated mixtures of amorphous silicate, olivine, pyroxene, metal and sulfides (Stroud et al., 2013).

However, ALH 77307 (CO3.03) shows evidence for incipient thermal alteration in the form of 10 nm to 30 nm Fe-rich rims on sub-micron matrix olivine grains (Brunner and Brearley, 2011), and amorphous Mg-Fe silicates, and minor, localized aqueous alteration in the form of layered silicates of a few nanometers in size (Stroud et al., 2013). In DOM 08006 there is some evidence for mobilization of Cr (chrome-spinel sub-grains in pyroxene; Fig. 8), but no Fe-rich rims were observed indicating that thermal metamorphism was very limited (Suppl. Figs. 5 and 6) (Stroud et al., 2013). The minor oxidation of amorphous silicates in DOM 08006 observed by Bonato et al. (2018) may result from the low degree of aqueous alteration experienced by this sample. The presence of Fe oxy-hydride needles in the matrix of DOM 08006 may result from terrestrial weathering (Fig. 2b), although it cannot be ruled out that some hydroxides may have formed in the CO parent body.

4.2.2. Opaque minerals

Opaque minerals alter at lower temperatures than silicate minerals and are thus more sensitive indicators of alteration (e.g., McCoy et al., 1999; Kimura et al., 2008). The relationship between Co and Ni in Ni-rich and Ni-poor metal is a sensitive indicator of the degree of thermal metamorphism experienced by a host meteorite in its parent body; a positive relationship indicates no noticeable heating (type $\ll$3.05), while an inverse or no relationship indicates thermal alteration above a type 3.05 (Kimura et al., 2008). Nickel-rich metal in DOM 08006 is enriched in Co relative to Ni-poor metal, similar to observations of metal in thermally unmetamorphosed ordinary and CO chondrites (including ALH 77307) (Fig. 5a; Kimura et al., 2008), indicating that the metal in DOM 08006 has experienced very little thermal metamorphism. This positive Co vs. Ni relationship is exhibited by Fe,Ni metal in unmetamorphosed carbonaceous chondrites from other groups, including the CR chondrites MET 00426 and QUE 99177 (Schrader et al., 2015), and MIL 090657 (Davidson et al., 2015; Davidson et al., 2019), and the ungrouped Acfer 094 (Kimura et al., 2008).

Chrome-spinel grains are very robust to aqueous alteration but alter during thermal metamorphism; while chrome-spinel grains from equilibrated and high petrologic type 3 chondrites are exclusively subhedral to anhedral, those from unequilibrated chondrites of low petrologic type tend to be euhedral (Johnson and Prinz, 1991; Davidson et al., 2011). Chrome-spinel grains, when present in FeO-rich chondrules, are very euhedral (Figs. 2e,f and 4e,f), further demonstrating the thermally pristine nature of DOM 08006.

The mineralogies, morphologies, and compositions of sulfide assemblages within chondritic meteorites are indicators of both the conditions under which they formed (nebular or parent body) and whether they were modified in their parent bodies. The morphologies of sulfide assemblages indicate whether they formed by low-temperature aqueous alteration or solid state exsolution (either at high or low temperature); pentlandite lamellae within pyrrhotite indicate solid state exsolution and are inconsistent with formation via aqueous alteration. Fine-grained (submicron) sulfides are present throughout the matrix of DOM 08006 (Fig. 6b), but sulfides can reach up to ~150 μm in diameter (e.g., Mx1; Fig. 4g). There is no evidence that any sulfides in either the matrix or chondrules were formed aqueously, and sulfide geothermometry (via Fe-Ni-S isothermal phase diagrams; Fig. 5b,c) suggests formation in the nebula at <400 °C (Fig. 5b and c).

As previously mentioned, at least some metal has been altered to magnetite in both chondrules and interchondrule matrix, indicating that minor aqueous alteration has taken place. However, since substantial amounts of metal remain (up to ~18 vol.% in FeO-poor chondrules; Table 4), this alteration was not extensive.

4.2.3. Silicate minerals

Beyond determining the Cr-contents of ferroan olivine (as discussed in Section 4.1), it is possible to use silicate

minerals to gauge the degree of parent body thermal metamorphism experienced by a chondrite using the Fe number or Fe# (i.e., Fe/[Fe + Mg] × 100) of olivine and low-Ca pyroxene in individual chondrules (e.g., Tenner et al., 2015; Schrader et al., 2017). Since Fe and Mg diffuse at different rates in olivine and pyroxene (Ganguly and Tazzoli, 1994; Chakraborty, 1997), olivine has higher Fe content (i.e., relatively higher Fe#) than pyroxene (i.e., lower Fe#) in thermally altered chondrites (e.g., Wlotzka, 2005). Chondrule data from DOM 08006 show a ~ 1:1 Fa/Fs ratio within 1σ error (Table 4; N.B., Fa is equivalent to Fe# for olivine, and in the case of low-Ca pyroxene reported here Fs was identical to Fe#, therefore the Fs values reported in Table 4 can be considered as representative of Fe#), similar to what is seen in minimally altered CR2 chondrites (e.g., Davidson et al., 2015; Davidson et al., 2019; Tenner et al., 2015; Schrader et al., 2017).

Compared to terrestrial plagioclase, lunar plagioclase exhibits anomalous stoichiometry, which has been attributed to the presence of "excess silica" denoted here as [ ] Si_4O_8 (Beaty and Albee, 1980). Experiments show that up to 10 wt.% silica can be incorporated into plagioclase at temperatures of 1200–1500 °C and 1 atm pressure under anhydrous conditions (Longhi and Hays, 1979). The lack of [ ]Si_4O_8 in terrestrial plagioclase compared to lunar plagioclase has been attributed to the presence of water, which lowers the liquidus temperatures (Beaty and Albee, 1980). Silica excesses have been reported for chondrule plagioclase from chondrites of low petrographic type (Tenner et al., 2014, Chaumard et al., 2017; Tenner, 2017). Carbonaceous chondrites of petrologic types CO3.05–3.1 and CV3.1 exhibit systematically lower An# and [ ]Si_4O_8 compared to the relatively more primitive ungrouped Acfer 094 and CR chondrites (Chaumard et al., 2017). Therefore, determining the degree of silica excess (or lack thereof) in chondrule plagioclase can be used as a measure of the degree of reheating experienced by these chondrites in their parent bodies (Tenner et al., 2014, Chaumard et al., 2017; Tenner, 2017).

Calculated excess silica abundances for plagioclase grains in 11 chondrules (10 FeO-poor, one FeO-rich) range from –1.8 mol.% to 6.9 mol.%; the plagioclase grains in five of the chondrules (all FeO-poor) show resolvable excess silica. The chondrules analyzed here in DOM 08006 exhibit a slightly wider range of excess silica than previously seen in a study of 33 chondrules (11 of which exhibited excess silica) from this same meteorite (–1.3 mol.% to 4.5 mol.%; Tenner, 2017). These results indicate that many DOM 08006 chondrules have experienced minimal, if any, reprocessing. Since parent body heating would require all chondrules to be affected, and this is not the case, the chondrules that do not exhibit excess silica in their chondrule plagioclase were likely reprocessed in the nebula. Alternatively, it may be that not all chondrule plagioclase incorporates excess silica. Nevertheless, the presence of excess silica in some plagioclase from DOM 08006 chondrules further reflects the primitive nature of this meteorite.

4.3. DOM 08006: Primitiveness demonstrated via noble gases

Trapped noble gas concentrations can be used to assess metamorphic grade within a class of meteorites. This works best for ordinary chondrites with large petrologic type differences (e.g., Anders and Zadnik, 1985; Sears et al., 1980). More subtle differences, on the order of 0.1 petrologic type increments, in type 3 CO chondrites are more difficult to detect. This is due to complicating factors, such as sample heterogeneity (trapped gases are expected entirely in the matrix and chondrule-matrix ratios vary throughout some samples) and terrestrial weathering (which mostly affects Kr and Xe). Typical masses suitable for bulk total noble gas extractions in primitive carbonaceous chondrites are ~5–20 mg. This is not necessarily sufficiently representative for a given meteorite (e.g., ~1 g is considered representative for bulk H-C-N analyses; Alexander et al., 2013). The sample analyzed here was an aliquot taken from powder of much larger (~1 g) bulk sample, but this is not the case for most literature data, where powdered bulk sample masses of <20 to 170 mg are commonly used.

Comparison of the trapped Ar-Xe concentrations in six CO3 *falls* (petrologic types 3.1–3.6) did not yield an obvious trend with metamorphic grade (Bartoschewitz et al., 2010). However, the DOM 08006 sample measured here has the highest concentrations of trapped ^{36}Ar and ^{132}Xe of all CO chondrites (cf. Mazor et al., 1970; Wieler et al., 1985; Scherer and Schultz, 2000; Bartoschewitz et al., 2010), supporting the suggestion that DOM 08006 is one of the most primitive chondrites known. The ^{84}Kr concentration, a product of terrestrial weathering, is higher in DOM 08006 than in most CO chondrites, apart from three Dar al Gani desert CO chondrite finds (Scherer and Shultz, 2000), illustrating the impact of terrestrial weathering.

Sample heterogeneity (e.g., chondrule-matrix ratios) can be compensated for by looking at elemental ratios. However, the Ar/Xe and Kr/Xe ratios from DOM 08006 are not as high as expected compared to other CO chondrites. This likely reflects the presence of a terrestrial Kr- and Xe-rich component in DOM 08006 acquired during terrestrial weathering in Antarctica, although the Xe contamination of the IOM could have occurred during demineralization. In contrast, the bulk $^{40}Ar/^{36}Ar$ ratio in DOM 08006 is 0.7, which is extremely low for bulk meteorites and excludes any significant contribution from terrestrial Ar ($^{40}Ar/^{36}Ar$ ~ 296). Therefore, when including finds from cold and hot deserts, the best parameter to assess the metamorphic grade of CO chondrites is the trapped ^{36}Ar concentration. DOM 08006 shows the highest ^{36}Ar concentration of all analyzed CO chondrites, including ALH 77307 (CO3.03) (Mazor et al., 1970; Wieler et al., 1985; Scherer and Schultz, 2000; Bartoschewitz et al., 2010), and hence appears to be the most primitive CO chondrite based on noble gas content.

Noble gases in IOM ("HF-HCl-resistant residues") also reflect the degree of thermal metamorphism and aqueous alteration experienced on a parent body (e.g., Busemann et al., 2000). Due to difficulties obtaining a meaningful mass (all of the noble gas carriers summed up may still only

contribute a small mass fraction to the IOM), these authors mostly compared element ratios. Comparing the $^{36}Ar/^{132}Xe$ and $^{84}Kr/^{132}Xe$ ratios of DOM 08006 IOM (0.409 ± 0.014 and 30.2 ± 1.3, respectively) with the literature data (cf. Busemann et al., 2000, Fig. 8) would lead to the conclusion that DOM 08006 is more thermally processed than all other CO chondrites analyzed (Kainsaz, Ornans, Lancé, Isna) and even type 3.6 and 3.7 ordinary chondrites, in direct contradiction of all other data presented here. However, the Xe isotopic composition of DOM 08006 (see Section 3.3) suggests a large terrestrial Xe contribution in the IOM (~2/3 of the detected Xe). This is supported by the high ^{132}Xe concentration of $(43.3 \pm 1.3) \times 10^{-8}$ cm^3 STP/g residue (higher than found in any other residue even including CM2 chondrites, Busemann et al., 2000), which is explained by addition of terrestrial Xe. Therefore, the ^{36}Ar concentration is the most insightful parameter here.

We can roughly determine the concentrations of Ne-E (its subcomponents cannot be resolved here) and Ne-HL using the mass fraction of 1.45 wt.% of IOM extracted from DOM 08006 (Alexander et al., 2018). Decomposing the measured IOM-Ne yields (in 10^{-10} cm^3/g) $\sim 3.1 \pm 0.3$ ^{22}Ne-E and $\sim 40.5 \pm 0.4$ ^{22}Ne-HL. This can be compared with concentrations found for HCl-HF-resistant residues (Huss et al. 2003, Table 5, Ne-E(H) and Ne-A2, which is Ne-HL including P6) of ALH 77307 (1.0 ± 2.5 and 34 ± 15, respectively) and Colony (1.1 ± 0.3 and 20.4 ± 2.4, respectively). Again, this illustrates the highly primitive nature of DOM 08006.

4.4. DOM 08006: A comparison with other studies

Presolar SiC abundances are affected by heating in some carbonaceous chondrite groups (Davidson et al., 2014a). DOM 08006 has a presolar SiC abundance ($35 + 27/-17$ ppm, 2σ; Nittler et al., 2018) that is comparable to those seen in other primitive chondrites (~30 ppm Davidson et al., 2014a) and higher than that reported for ALH 77307 (11 ppm + 4/–3 ppm; Davidson et al., 2014a). Oxygen-rich presolar silicate grains are destroyed by parent body processes (either thermal or aqueous) (e.g., Floss and Haenecour, 2016 and references therein). DOM 08006 has an extremely high presolar O-rich grain (silicate and oxide) abundance ($257 + 76/-96$ ppm, 2σ; Nittler et al., 2013, 2018), which is higher than those from the CO3.03 ALH 77307 (188 ppm; Nguyen et al., 2010) and the primitive ungrouped chondrite Acfer 094 (189 ppm; Vollmer et al., 2009). These high presolar grain abundances further demonstrate the minimally altered nature of DOM 08006. This agrees with the observation that the CAIs in DOM 08006 are also very primitive, similar to those seen in Acfer 094 (Simon and Grossman, 2015).

Since the bulk C contents of chondrites decrease with increasing thermal metamorphism, bulk C abundances and isotopic compositions can be useful indicators of petrologic type (e.g., Alexander et al., 2012, 2013, 2018). DOM 08006 has a higher bulk C content and D/H and $^{15}N/^{14}N$ ratios than any other CO measured to date, including ALH 77307, suggesting that it preserves more primitive organics and is less metamorphosed (Alexander et al., 2018). As the major C-bearing component in chondrites, IOM is a sensitive indicator of metamorphism; as metamorphism progresses IOM becomes less abundant and more 'graphitic' (e.g., Quirico et al., 2003; Alexander et al., 2007; Bonal et al., 2007) and its C isotopic composition changes (e.g., Alexander et al., 2018). Bulk H abundances and isotopes are also useful indicators of the degree of aqueous alteration experienced in carbonaceous chondrites (Alexander et al., 2013). The higher H/C ratio of IOM isolated from DOM 08006 indicates that it is more primitive than ALH 77307 and other CO chondrites, but similar to LL3.00 Semarkona (Alexander et al., 2018). Indeed, a Raman spectroscopic study of IOM extracted from DOM 08006 showed that the structural order of the polyaromatic carbonaceous matter (which becomes progressively more ordered during thermal metamorphism) was lower than in ALH 77307 (Bonal et al., 2016), further demonstrating that DOM 08006 is of petrologic type 3.00 and more primitive than ALH 77307 (CO3.03).

4.5. DOM 08006: Links with other chondrites and chondrite groups

Although DOM 08006 was tentatively paired with DOM 08004 (Weisberg et al., 2010), the two appear to be somewhat different in terms of their bulk C abundances (DOM 08006 has a higher bulk C abundance) and H-C-N isotopic compositions (Alexander et al., 2018). While DOM 08004 was not studied here, DOM 10104 from the same pairing group was; these two meteorites have similar bulk C abundances and H-C-N isotopic compositions (Alexander et al., 2018). In terms of Cr-content of ferroan olivine, DOM 10104 appears to be more thermally metamorphosed than DOM 08006, suggesting that they are not paired.

Simon and Grossman (2015) noted that the CAIs of DOM 08006 and DOM 08004 appear to be more Acfer 094-like than CO3-like. This was based on high abundances of inclusions containing the highly refractory mineral grossite, the presence of FeO-enrichments, and the occurrence of rims on many CAIs (Simon and Grossman, 2015). Though Simon and Grossman (2015) suggested that DOM 08004, DOM 08006 and Acfer 094 be considered a subgroup of CO3 chondrites, these three meteorites are significantly different in terms of bulk isotopic compositions (Alexander et al., 2018), the nature of their IOM (e.g., Bonal et al., 2016; Alexander et al., 2018), and their noble gases (Acfer 094 contains far greater trapped ^{36}Ar than DOM 08006; Scherer and Schultz, 2000). We suggest that DOM 08006 is a CO chondrite of petrologic type 3.00.

5. SUMMARY

The five CO3 chondrites analyzed here appear to complete the CO3.00–3.2 metamorphic trend initially defined by Grossman and Brearley (2005) based on the Cr-content of ferroan olivine, providing a useful tool for determining the relative degree of thermal metamorphism experience by CO chondrites of low petrologic type (CO3.00 to 3.2).

DOM 08006 appears to be one of the most, if not the most, primitive carbonaceous chondrites analyzed to date, as reflected by its matrix mineralogy, opaque mineralogy, Co/Ni ratios of its Fe,Ni metal, the Cr-content of its ferroan olivine, the Fe# ratio of olivine and low-Ca pyroxene in its chondrules, the presence of excess silica in chondrule plagioclase, and the high abundance of ^{36}Ar and ^{132}Xe noble gases. While DOM 08006 has experienced some terrestrial weathering and limited aqueous alteration on its parent body (as seen by the presence of magnetite and high ^{84}Kr concentration), it exhibits virtually no evidence for thermal metamorphism. This conclusion agrees with that derived from presolar grain abundances (Nittler et al., 2018), bulk C-abundances and isotopic compositions (Alexander et al., 2018), and Raman spectroscopy (Bonal et al., 2016). DOM 08006 appears to be a CO3.00. The minimally altered nature of DOM 08006 demonstrates that it is an extremely important sample for providing valuable insight into early Solar System conditions. At a total weight of 667 g, a significant amount of primitive material is available for a wide array of future studies.

ACKNOWLEDGEMENTS

We thank J. T. Armstrong for assistance with the electron microprobe. US Antarctic meteorite samples are recovered by the Antarctic Search for Meteorites (ANSMET) program, which has been funded by NSF and NASA, and characterized and curated by the Department of Mineral Sciences of the Smithsonian Institution and the Astromaterials Acquisition and Curation Office at NASA Johnson Space Center. This manuscript was significantly improved by helpful reviews from Emma Bullock, Ashley King, an anonymous reviewer, and the editorial expertise of AE Sara Russell. This work was funded by NASA grants NNX11AG67G (PI: CMODA), NNX10AI63G and NNX11AB40G (PI: LRN), and NNH09AL20I (PI: RMS), and by the Swiss National Science Foundation through the NCCR "PlanetS" (HB).

APPENDIX A. SUPPLEMENTARY MATERIAL

Supplementary data to this article can be found online at https://doi.org/10.1016/j.gca.2019.08.032.

REFERENCES

Abreu N. M. and Brearley A. J. (2010) Early solar system processes recorded in the matrices of two highly pristine CR3 carbonaceous chondrites, MET 00426 and QUE 99177. *Geochim. Cosmochim. Acta* **74**, 1146–1171.

Alaerts L., Lewis R. S. and Anders E. (1979a) Isotopic anomalies of noble gases in meteorites and their origins – III. LL-chondrites. *Geochim. Cosmochim. Acta* **43**, 1399–1415.

Alaerts L., Lewis R. S. and Anders E. (1979b) Isotopic anomalies of noble gases in meteorites and their origins – IV. C3 (Ornans) carbonaceous chondrites. *Geochim. Cosmochim. Acta* **43**, 1421–1432.

Alexander C. M. O'D., Fogel M., Yabuta H. and Cody G. D. (2007) The origin and evolution of chondrites recorded in the elemental and isotopic compositions of their macromolecular organic matter. *Geochim. Cosmochim. Acta* **71**, 4380–4403.

Alexander C. M. O'D., Newsome S. D., Fogel M. L., Nittler L. R., Busemann H. and Cody G. D. (2010) Deuterium enrichments in chondritic macromolecular material – Implications for the origin and evolution of organics, water and asteroids. *Geochim. Cosmochim. Acta* **74**, 4417–4437.

Alexander C. M. O'D., Bowden R., Fogel M. L., Howard K. T., Herd C. D. K. and Nittler L. R. (2012) The provenances of asteroids, and their contributions to the volatile inventories of the terrestrial planets. *Science* **337**, 721–723.

Alexander C. M. O'D., Howard K. T., Bowden R. and Fogel M. L. (2013) The classification of CM and CR chondrites using bulk H, C, and N abundances and isotopic compositions. *Geochim. Cosmochim. Acta* **123**, 244–260.

Alexander C. M. O'D., Bowden R. and Howard K. T. (2014) A multi-technique search for the most primitive CO chondrites. Lunar Planet. Sci. XLV. Lunar Planet. Inst., Houston. #2667 (abstr.).

Alexander C. M. O'D., Greenwood R. C., Bowden R., Gibson J. M., Howard K. T. and Franchi I. A. (2018) A multi-technique search for the most primitive CO chondrites. *Geochim. Cosmochim. Acta* **221**, 406–420.

Amari S., Lewis R. S. and Anders E. (1995) Interstellar grains in meteorites: III. Graphite and its noble gases. *Geochim. Cosmochim. Acta* **59**, 1411–1426.

Anders E. and Zadnik G. (1985) Unequilibrated ordinary chondrites: A tentative subclassification based on volatile-element content. *Geochim. Cosmochim. Acta* **49**, 1281–1291.

Bartoschewitz R., Ott U., Franke L., Herrmann S., Yamamoto Y., Nagao K., Bilet M. and Grau T. (2010) Noble gas record and cosmic-ray exposure history of the new CO3 chondrite Moss - Comparison with Lancé and other CO chondrite falls. *Meteorit. Planet. Sci.* **45**, 1380–1391.

Beaty D. W. and Albee A. L. (1980) Silica solid solution and zoning in natural plagioclase. *Am. Mineral.* **65**, 63–74.

Bonal L., Bourot-Denise M., Quirico E., Montagnac G. and Lewin E. (2007) Organic matter and metamorphic history of CO chondrites. *Geochim. Cosmochim. Acta* **71**, 1605–1623.

Bonal L., Quirico E., Flandinet L. and Montagnac G. (2016) Thermal history of type 3 chondrites from the Antarctic meteorite collection determined by Raman spectroscopy of their polyaromatic carbonaceous matter. *Geochim. Cosmochim. Acta* **189**, 312–337.

Bonato E., King A. J., Schofield P. F., Kaulich B., Araki T., Kazemian M., Lee M. R. and Russell S. S. (2019) In-situ carbon, nitrogen, and oxygen XANES analysis of the matrix in pristine CO3 carbonaceous chondrites. Lunar Planet. Sci. L. Lunar Planet. Inst., Houston. #3047(abstr.).

Bonato E., King A. J., Schofield P. F., Kaulich B., Araki T., Abyaneh M. K., Lee M. R. and Russell S. S. (2018) The oxidation state of iron in silicate minerals from the matrices of CO carbonaceous chondrites. Lunar Planet. Sci. XLIX. Lunar Planet. Inst., Houston. #1917(abstr.).

Brearley A. J. (1993) Matrix and fine-grained rims in the unequilibrated CO3 chondrite, ALH77307 – Origins and evidence for diverse, primitive nebular dust components. *Geochim. Cosmochim. Acta* **57**(7), 1521–1550.

Brunner C. E. and Brearley A. J. (2011) TEM study of matrix in the CO3 chondrite ALHA 77307: Clues about the first stages of metamorphism in chondrites. *Meteorit. Planet. Sci. Supp.* **#5403** (abstr.).

Burton A. S., Elsila J. E., Callahan M. P., Martin M. G., Glavin D. P., Johnson N. M. and Dworkin J. P. (2012) A propensity for n-ω-amino acids in thermally altered Antarctic meteorites. *Meteorit. Planet. Sci.* **47**, 374–386.

Busemann H., Baur H. and Wieler R. (2000) Primordial noble gases in "phase Q" in carbonaceous and ordinary chondrites studied by closed-system stepped etching. *Meteorit. Planet. Sci.* **35**, 949–973.

Busemann H., Young A. F., Alexander C. M. O'D., Hoppe P., Mukhopadhyay S. and Nittler L. R. (2006) Interstellar chemistry recorded in organic matter from primitive meteorites. *Science* **312**, 727–730.

Chakraborty S. (1997) Rates and mechanisms of Fe-Mg interdiffusion in olivine at 980–1300°C. *J. Geophys. Res.* **102**, 12317–12331.

Chaumard N., Hertwig A. T., Kita N. T., Tenner T. J. and Kimura M. (2017) Measurements of silica excess in plagioclase in chondrules from primitive carbonaceous chondrites: Implications for 26Al–26Mg systematics. 80th Annual Meeting of the Meteoritical Society, #6309 (abstr.).

Craig J. R., Naldrett A. J. and Kullerud G. (1968) The Fe–Ni–S system: 400°C isothermal diagram. *Carnegie I. Wash.* **66**, 440–441.

Davidson J., Lauretta D. S. and Schrader D. L. (2011) Textural and compositional variations in chromites from reduced CV3 chondrites. *Meteorit. Planet. Sci. Supp.* **#5319** (abstr.).

Davidson J., Busemann H., Nittler L. R., Alexander C. M. O'D., Orthous-Daunay F.-R., Franchi I. A. and Hoppe P. (2014a) Abundances of presolar silicon carbide grains in primitive meteorites determined by NanoSIMS. *Geochim. Cosmochim. Acta* **139**, 248–266.

Davidson J., Nittler L. R., Alexander C. M. O'D. and Stroud R. N. (2014b) Petrography of very primitive CO3 chondrites: Dominion Range 08006, Miller Range 07687 and four others. Lunar Planet. Sci. XLV. Lunar Planet. Inst., Houston. #1384 (abstr.).

Davidson J., Alexander C. M. O'D., Schrader D. L., Nittler L. R. and Bowden R. (2015) Miller Range 090657: A very pristine Renazzo-like (CR) carbonaceous chondrite. Lunar Planet. Sci. XLVI. Lunar Planet. Inst., Houston. #1603(abstr.).

Davidson J., Schrader D. L., Alexander C. M. O'D., Nittler L. R. and Bowden R. (2019) Re-examining thermal metamorphism of the Renazzo-like (CR) carbonaceous chondrites: Insights from pristine Miller Range 090657 and shock-heated Graves Nunataks 06100. *Geochim. Cosmochim. Acta*, in press.

Eugster O. (1988) Cosmic-ray production rates for ^{3}He, ^{21}Ne, ^{38}Ar, ^{83}Kr, and ^{126}Xe in chondrites based on ^{81}Kr-Kr exposure ages. *Geochim. Cosmochim. Acta* **52**, 1649–1662.

Floss C. and Haenecour P. (2016) Presolar silicate grains: abundances, isotopic and elemental compositions, and the effects of secondary processing. *Geochem. J.* **50**, 3–15.

Floss C. and Stadermann F. (2009) High abundances of circumstellar and interstellar C-anomalous phases in the primitive CR3 chondrites QUE 99177 and MET 00426. *Astrophys. J.* **697**, 1242–1255.

Ganguly J. and Tazzoli V. (1994) Fe2+-Mg interdiffusion in orthopyroxene: Retrieval from the data on intracrystalline exchange reaction. *Am. Mineral.* **79**, 930–937.

Greshake A. (1997) The primitive matrix components of the unique carbonaceous chondrite Acfer 094: A TEM study. *Geochim. Cosmochim. Acta* **61**(2), 437–452.

Grossman J. N. and Brearley A. J. (2005) The onset of metamorphism in ordinary and carbonaceous chondrites. *Meteorit. Planet. Sci.* **40**, 87–122.

Grossman J. N. and Rubin A. E. (2006) Dominion Range 03238: A possible missing link in the metamorphic sequence of CO3 chondrites. Lunar Planet. Sci. XXXVII. Lunar Planet. Inst., Houston. #1383(abstr.).

Howard K. T., Alexander C. M. O'D., Schrader D. L. and Dyl K. A. (2015) Classification of hydrous meteorites (CR, CM and C2 ungrouped) by phyllosilicate fraction: PSD-XRD modal mineralogy and planetesimal environments. *Geochim. Cosmochim. Acta* **149**, 206–222.

Huss G. R. and Lewis R. S. (1994) Noble gases in presolar diamonds I: Three distinct components and their implications for diamond origins. *Meteoritics* **29**, 791–810.

Huss G. R., Meshik A. P., Smith J. B. and Hohenberg C. M. (2003) Presolar diamond, silicon carbide, and graphite in carbonaceous chondrites: Implications for thermal processing in the solar nebula. *Geochim. Cosmochim. Acta* **67**, 4823–4848.

Johnson C. A. and Prinz M. (1991) Chromite and olivine in type II chondrules in carbonaceous and ordinary chondrites: Implications for thermal histories and group differences. *Geochim. Cosmochim. Acta* **55**, 893–904.

Jones R. H. (1992) On the relationship between isolated and chondrule olivine grains in the carbonaceous chondrite ALHA77307. *Geochim. Cosmochim. Acta* **56**, 467–482.

Kimura M., Grossman J. N. and Weisberg M. K. (2008) Fe-Ni metal in primitive chondrites: Indicators of classification and metamorphic conditions for ordinary and CO chondrites. *Meteorit. Planet. Sci.* **43**, 1161–1177.

Kosyakov V. I., Sinyakova E. F. and Shestakov V. A. (2003) Dependence of sulphur fugacity on the composition of phase associations in the Fe–FeS–NiS–Ni system at 873 K. *Geochem. Int.* **7**, 660–669.

Krietsch D., Busemann H., Riebe M. E. I., King A. J. and Maden C. (2019) Complete characterization of the noble gas inventory in CR chondrite Miller Range 090657 by direct etch release. 82nd Annual Meeting of the Meteoritical Society, #6296 (abstr.).

Lewis R. S., Amari S. and Anders E. (1994) Interstellar grains in meteorites: II. SiC and its noble gases. *Geochim. Cosmochim. Acta* **58**, 471–494.

Leya I. and Masarik J. (2009) Cosmogenic nuclides in stony meteorites revisited. *Meteorit. Planet. Sci.* **44**, 1061–1086.

Lodders K. and Fegley, Jr., B. (1998) *The Planetary Scientist's Companion*. Oxford University Press, New York.

Lodders K., Palme H. and Gail H.-P. (2009) Abundances of the elements of the solar system. In *The Landolt-Bornstein Database* (ed. J. E. Trümper). Springer, Berlin, pp. 560–598.

Longhi J. and Hays J. F. (1979) Phase equilibria and solid solution along the join $CaAl_2Si_2O_8$–SiO_2. *Am. J. Sci.* **279**, 876–890.

Matsuda J.-I., Lewis R. S., Takahashi H. and Anders E. (1980) Isotopic anomalies of noble gases in meteorites and their origins - VII. C3V carbonaceous chondrites. *Geochim. Cosmochim. Acta* **44**, 1861–1874.

Mazor E., Heymann D. and Anders E. (1970) Noble gases in carbonaceous chondrites. *Geochim. Cosmochim. Acta* **34**, 781–824.

McCoy T. J., Dickinson T. L. and Lofgren G. E. (1999) Partial melting of the Indarch (EH4) meteorite: A textural, chemical and phase relations view of melting and melt migration. *Meteorit. Planet. Sci.* **34**, 735–746.

McSween, Jr., H. Y. (1977) Carbonaceous chondrites of the Ornans type: a metamorphic sequence. *Geochim. Cosmochim. Acta* **41**, 477–491.

Nagashima K., Krot A.N. and Park C. (2015) An amoeboid olivine aggregate surrounded by an igneous ferroan olivine-rich rim from CO3.0 chondrite DOM 08006. Lunar Planet. Sci. XLVI. Lunar Planet. Inst., Houston. #2477(abstr.).

Newton J., Bischoff A., Arden J. W., Franchi I. A., Geiger T., Greshake A. and Pillinger C. T. (1995) Acfer 094, a uniquely primitive carbonaceous chondrite from the Sahara. *Meteoritics* **30**, 47–56.

Nguyen A. N., Stadermann F. J., Zinner E., Stroud R. M., Alexander C. M. O'D. and Nittler L. R. (2007) Characterization of presolar silicate and oxide grains in primitive carbonaceous chondrites. *Astrophys. J.* **656**, 1223–1240.

Nguyen A. N., Nittler L. R., Stadermann F. J., Stroud R. M. and Alexander C. M. O'D. (2010) Coordinated analyses of presolar grains in the Allan Hills 77307 and Queen Elizabeth Range 99177 meteorites. *Astrophys. J.* **719**, 166–189.

Nittler L. R., Alexander C. M. O'D. and Stroud R. M. (2013) High abundance of presolar materials in CO3 chondrite Dominion Range 08006. Lunar Planet. Sci. XLIV. Lunar Planet. Inst., Houston. #2367(abstr.).

Nittler L. R., Alexander C. M. O'D., Davidson J., Riebe M. E. I., Stroud R. M. and Wang J. (2018) High abundances of presolar grains and ^{15}N-rich organic matter in CO3.0 chondrite Dominion Range 08006. *Geochim. Cosmochim. Acta* **226**, 107–131.

Ott U. (2014) Planetary and pre-solar noble gases in meteorites. *Geochemistry* **74**, 519–544.

Quirico E., Raynal P. I. and Bourot-Denise M. (2003) Metamorphic grade of organic matter in six unequilibrated ordinary chondrites. *Meteorit. Planet. Sci.* **38**, 795–811.

Raghavan V. (2004) Fe–Ni–S (iron–nickel–sulfur). *J. Phase Equilib.* **25**, 373–381.

Riebe M. E. I., Welten K. C., Meier M. M. M., Wieler R., Bart M. I. F., Ward D., Laubenstein M., Bischoff A., Caffee M. W., Nishiizumi K. and Busemann H. (2017) Cosmic-ray exposure ages of six chondritic Almahata Sitta fragments. *Meteorit. Planet. Sci.* **52**, 2353–2374.

Rubin A. E. (1989) Size-frequency distributions of chondrules in CO3 chondrites. *Meteoritics* **24**, 179–189.

Rubin A. E. (2000) Petrologic, geochemical and experimental constraints on models of chondrule formation. *Earth Sci. Rev.* **50**, 3–27.

Rubin A. E. (2010) Physical properties of chondrules in different chondrite groups: Implications for multiple melting events in dusty environments. *Geochim. Cosmochim. Acta* **74**, 4807–4828.

Scherer P. and Schultz L. (2000) Noble gas record, collisional history, and pairing of CV, CO, CK and other carbonaceous chondrites. *Meteorit. Planet. Sci.* **35**, 145–153.

Schneider C. A., Rasband W. S. and Eliceiri K. W. (2012) NIH Image to ImageJ: 25 years of image analysis. *Nat. Methods* **9**, 671–675.

Schrader D. L. and Davidson J. (2017) CM and CO chondrites: A common parent body or asteroidal neighbors? Insights from chondrule silicates. *Geochim. Cosmochim. Acta* **214**, 157–171.

Schrader D. L., Connolly, Jr., H. C., Lauretta D. S., Zega T. J., Davidson J. and Domanik K. J. (2015) The formation and alteration of the Renazzo-like carbonaceous chondrites III: Towards understanding the genesis of ferromagnesian chondrules. *Meteorit. Planet. Sci.* **50**, 15–50.

Schrader D. L., Nagashima K., Krot A. N., Ogliore R. C., Yin Q.-Z., Amelin Y. A., Stirling C. H. and Kaltenbach A. (2017) Distribution of ^{26}Al in the CR chondrite chondrule-forming region of the protoplanetary disk. *Geochim. Cosmochim. Acta* **201**, 275–302.

Scott E. R. D. and Jones R. H. (1990) Disentangling nebular and asteroidal features of CO3 carbonaceous chondrite meteorites. *Geochim. Cosmochim. Acta* **54**, 2485–2502.

Scott E. R. D. and Krot A. N. (2005) Chondritic meteorites and the high-temperature nebular origins of their components. In *Chondrites and the Protoplanetary Disk* (eds. A. N. Krot, E. R. D. Scott and B. Reipurth). ASP Conference Series, pp. 15–53.

Sears D. W., Grossman J. N., Melcher C. L., Ross L. M. and Mills A. A. (1980) Measuring metamorphic history of unequilibrated ordinary chondrites. *Nature* **287**, 791–795.

Simon S. B. and Grossman L. (2011) Refractory inclusions in the unique carbonaceous chondrite Acfer 094. *Meteorit. Planet. Sci.* **46**, 1197–1216.

Simon S. B. and Grossman L. (2015) Refractory inclusions in the pristine carbonaceous chondrites DOM 08004 and DOM 08006. *Meteorit. Planet. Sci.* **50**, 1032–1049.

Stroud R. M., Nittler L. R. and Alexander C. M. O'D. (2013) Analytical electron microscopy of a CAI-Like presolar grain and associated fine-grained matrix materials in the Dominion Range 08006 CO3 meteorite. Lunar Planet. Sci. XLIV. Lunar Planet. Inst., Houston. #2315(abstr.).

Tenner T. J. (2017) Evaluating silica excess in Dominion Range 08006 chondrule plagioclase: Comparisons to Yamato 81020 and Acfer 094 chondrule plagioclase. 80th Annual Meeting of the Meteoritical Society, #6394 (abstr.).

Tenner T. J., Ushikubo T., Nakashima D., Kita N. T., Weisberg M. K. and Kimura M. (2014) Silica excess in anorthitic plagioclase from type 3.00 chondrite chondrules: Evidence for retaining primary 26Al-26Mg systematics. Lunar Planet. Sci. XLV. Lunar Planet. Inst., Houston. #1187(abstr.).

Tenner T. J., Nakashima D., Ushikubo T., Kita N. T. and Weisberg M. K. (2015) Oxygen isotope ratios of FeO-poor chondrules in CR3 chondrites: Influence of dust enrichment and H_2O during chondrule formation. *Geochim. Cosmochim. Acta* **148**, 228–250.

Vollmer C., Hoppe P., Stadermann F. J., Floss C. and Brenker F. E. (2009) NanoSIMS analysis and Auger electron microscopy of silicate and oxide stardust from the carbonaceous chondrite Acfer 094. *Geochim. Cosmochim. Acta* **73**, 7127–7149.

Weisberg M. K., Smith C., Herd C., Haack H., Yamaguchi A., Chennaoui Aoudjehane H., Welzenbach L. and Grossman J. N. (2010) The Meteoritical Bulletin, No. 98, September 2010. *Meteorit. Planet. Sci.* **45**, 1530–1551.

Wieler R., Baur H., Graf T. and Signer P. (1985) He, Ne, and Ar in Antarctic meteorites: Solar noble gases in an enstatite chondrite. Lunar Planet. Sci. Conf. XVI. Lunar Planet. Inst., Houston. 902–903 (abstr.).

Wlotzka F. (2005) Cr spinel and chromite as petrogenetic indicators in ordinary chondrites: Equilibration temperatures of petrologic types 3.7 to 6. *Meteorit. Planet. Sci.* **40**, 1673–1702.

Zinner E. (2014) Presolar grains. In *Meteorites and Cosmochemical Processes, Volume 1 of Treatise on Geochemistry, Second Edition* (ed. A. M. Davis). Elsevier, pp. 181–213.

Associate editor: Sara S. Russell